

Timing, Synchronization & Longitudinal Aspects

H. Damerau

CERN, Geneva, Switzerland

Abstract

The transfer of beams from one accelerators to another requires a set of parameters correctly adjusted, as well as a sequence of events to trigger all elements relevant to the transfer exactly at the right moment with respect to the beam. The course introduces the basic building blocks of synchronization systems and beam synchronous timing generation. The parameters for the transfer are then derived starting from longitudinal beam dynamics. Furthermore, The steps for the transfer of lepton and hadron beams between circular accelerators are summarized.

Keywords

Longitudinal beam dynamics, beam synchronous timing, bunch-to-bucket transfer, beam synchronization, energy matching, longitudinal matching

1 Introduction

Synchronization is required every time two or more events must take place at the same time and at the same location. This is as true for people who would like to get together for a meeting, where nonetheless being late by few minutes is usually considered acceptable, as for particles beams which meet another beam or injection and ejection elements that have to be triggered for the beam transfer. The precision needed depends on the system considered. While two synchronized events may be millions of years apart in astronomy, particle beams travelling at a significant fraction of the speed of light require time precisions from nanoseconds down to few femtoseconds.

Table 1 gives the order of magnitude for the typical time scales, mostly defined by the length of the particle bunches. The technology for the synchronisation system must be chosen accordingly.

Table 1: Time scales of common accelerator types, mainly defined by their bunch length.

Proton bunches in low energy synchrotrons (few GeV)	> 10 ns
Proton bunches in medium energy synchrotrons	100 ns...1 ns
Bunch length in hadron colliders (> 100 GeV)	10 ns...100 ps
Electron storage rings	10 ps...1 ps
Plasma wakefield accelerators	1 ps...100 fs
Self Amplified Spontaneous Emission (SASE) FELs	1 ps...10 fs
Pump-probe FELs	< 100 fs
Jitter achievable with low-level RF electronics	10 ps...1 ps

While standard low-level RF electronics hardware is fully sufficient for hadron and circular electron accelerators, free-electron lasers with bunch lengths in the pico-second regime and below require optical synchronization techniques [1].

To illustrate the underlying principles and for the sake of simplicity this course focuses on standard techniques of synchronization and longitudinal transfer of beams, with particular attention to the transfer of bunched beams between two circular accelerators. The implementation is described only to the detail required to understand the concepts to synchronize beams, derive beam synchronous timings, achieve energy, as well as longitudinal matching.

Due to their low mass, leptons are extremely close to the speed of light in most accelerators. Already 99.99995 % of it are reached even in a small size electron synchrotron with an energy of only 500 MeV [2]. The oscillations of particles in the longitudinal and transverse directions are moreover damped by synchrotron radiation [3], forcing the particles to the longitudinal position enforced by the RF fields. In electron accelerators beam transfers are therefore fully deterministic in most cases. All signals for the RF systems and the triggers involved in the transfer are derived from a single master clock.

The fixed frequency approach is not possible in hadron accelerators where beam synchronous signals are derived from the circulating beam. The beam-based generation of RF signals is required to avoid longitudinal beam oscillations in the absence of synchrotron radiation. The exact moment of a beam transfer in absolute time hence depends on the beam itself and changes from acceleration cycle to cycle. Additionally, the RF frequency sweeps to track the increasing revolution frequency during acceleration.

Following the introduction of basic techniques and building blocks for beam transfer systems, the transfer between two circular accelerators is discussed. The longitudinal beam dynamics aspects are introduced in view of the transfer of bunched beams. Thereafter, the relevance of periodicity and bucket numbering is explained. The generation of trigger events for the beam transfer completes the requirements for electron accelerators. In hadron accelerators frequencies change and the target for a beam transfer can move in time. Additional difficulties are caused by the absence of synchrotron radiation damping. Strategies to match the beam energy and the longitudinal parameters are described to transfer hadrons with virtually no degradation of the longitudinal beam quality.

2 Techniques and building blocks

The basic techniques and building blocks of synchronization systems for beam transfer, in particular for large scale accelerator facilities, are introduced in what follows. Signals, either in the form of time marker pulses, RF signals, or as general timing infrastructure must be exchanged between accelerators involved in a beam transfer. The distances for these transmission can range up to several kilometers.

2.1 Signals with noise

The quality of any RF signal is degraded due to noise which leads to an unwanted variation of the signal phase or amplitude with time, the so-called jitter. In particular a phase variation, the phase jitter, introduces an uncertainty to the definition of phase and time information contained in the signal.

2.1.1 Coherent and incoherent signals

The difference between a coherent signal and noise is illustrated in Fig. 1. It shows the same signal

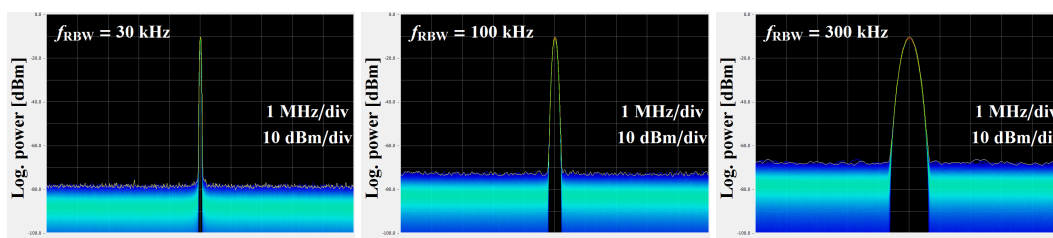


Fig. 1: Spectrum of an RF signal at 200 MHz measured with a resolution bandwidth, f_{RBW} of 30 kHz (left), 100 kHz (middle) and 300 kHz (right).

at 200 MHz measured with a spectrum analyser at three different resolution bandwidths. While the peak of the spectrum, representing the coherent part of the signal, is always at the same amplitude, the

noise level, as well as the width of the peak change proportionally to the observation bandwidth called resolution bandwidth, f_{RBW} , of the spectrum analyser.

Since the incoherent noise has a quasi-constant power density, i.e., power per bandwidth, the total power passing through the observation filter of the spectrum is proportional to its bandwidth. In case of the measurement shown in Fig. 1, the noise level is mainly dominated by the front-end amplifier and the mixer of the spectrum analyzer.

In the ideal case the thermal noise power density of a passive object at the temperature T is given by [4,5]

$$\frac{P}{\Delta f} = kT G(f) \quad \text{with} \quad G(f) = \frac{hf}{kT} / \left(e^{hf/kT} - 1 \right) .$$

The Boltzmann and Planck constants are k and h . In the relevant frequency and temperature range of electric signals on conductors, the form factor $G(f)$ can be approximated to one, since $hf/kT \ll 1$. At room temperature, $T \simeq 296$ K, the noise power density hence becomes $P/\Delta f \simeq kT = -174$ dBm/Hz.

2.1.2 Analysis of phase noise

The power spectrum of oscillator at the centre frequency, f_c , with phase jitter is sketched in Fig. 2. All

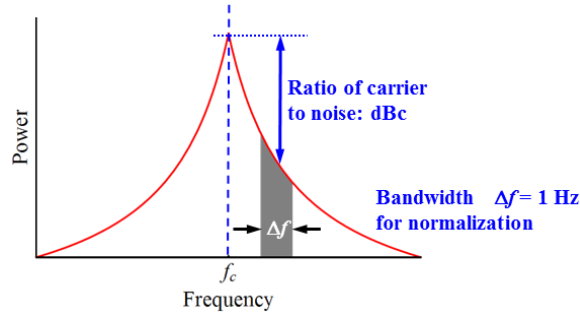


Fig. 2: Power spectrum of an oscillator signal at the frequency, f_c , with side-bands caused by noise.

power levels are defined as ratios with respect to the amplitude of the signal at the centre frequency, the carrier, in units of dBc. The noise power density is defined as the ratio of the power density and carrier power [6],

$$\mathcal{L}(f) = \frac{\text{Power density} \left[\frac{\text{dBc}}{\text{Hz}} \right]}{\text{Carrier power}} = \frac{1}{2} S_\phi(f) . \quad (1)$$

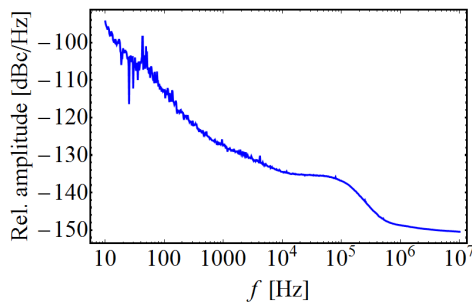
Integrating the noise power density Eq. (1) and using $\Delta t = \Delta\phi/(2\pi f_c)$ gives the RMS jitter of the signal

$$\Delta t_{\text{rms}} = \frac{1}{2\pi f_c} \sqrt{\int_{f_1}^{f_2} S_\phi(f) df} \quad (2)$$

in the frequency range from f_1 to f_2 . Seen that the noise power of most signals decreases with the frequency offset from the central frequency, the integration limits are conveniently given as offset frequencies from the carrier.

Fig. 3 (left) shows the phase noise density of a laboratory RF generator (Agilent/Keysight E8663B) at offset frequencies from 10 Hz to 10 MHz from the carrier at 1 GHz, together with the jitter per decade (Fig. 3, right). Due to the form of Eq. (2) the individual jitters per decade, $t_{\text{rms},n}$, can be added as a geometric sum such that the total jitter becomes

$$\Delta t_{\text{rms}} = \sqrt{\Delta t_{\text{rms},1}^2 + \Delta t_{\text{rms},2}^2 + \dots + t_{\text{rms},n}^2} .$$



Frequency range	Δt_{rms} [fs]
10 Hz. . . 100 Hz	12.4
100 Hz. . . 1 kHz	5.5
1 kHz. . . 10 kHz	5.5
10 kHz. . . 100 kHz	11.1
100 kHz. . . 1 MHz	13.0
1 MHz. . . 10 MHz	21.3
Total	31.0

Fig. 3: Phase noise density versus frequency offset (left) and RMS jitter per decade of frequency offset (right).

2.2 Transmission of RF signals over long distances

In large scale accelerator facilities reference signals must often be transmitted over distances of several kilometres, from one accelerator to another. Without taking any precautions, the thermal drift of such long coaxial cables or optical fibres may become significant with respect to the bunch length. The thermal coefficient of delay (TCD), defined as

$$\text{TCD} = \frac{\Delta\tau}{\tau} \cdot \frac{1}{\Delta T} = \frac{\Delta\phi}{\phi} \cdot \frac{1}{\Delta T},$$

as measured for a standard RG223 coaxial cable is plotted in Fig. 4. A 2 km long cable of this type

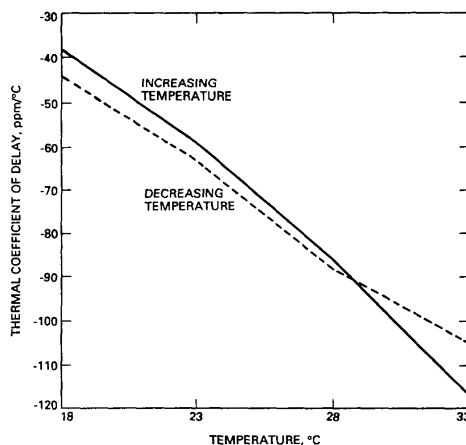


Fig. 4: Thermal coefficient of delay for an RG223 coaxial cable measured with increasing and decreasing temperature [7].

has about 10 μs delay. Changing the temperature by only 1 K at room temperature changes its delay by about 0.5 ns. This may be acceptable for the RF frequency as low as 10 MHz like in the Proton Synchrotron (PS) at CERN, but is certainly not in the case of the Large Hadron Collider (LHC), where the same delay would lead to a phase error of 73° at an RF frequency of about 400 MHz.

The thermal coefficient of delay for optical fibres is typically 10 to 100 times smaller compared to coaxial cables, but still the remaining drift may not be acceptable. The phase drift of a optical fibre with a length of about 6.3 km measured at a frequency of 200 MHz together with the temperature is shown in Fig. 5. Without compensation, the delay of the fibre changes by almost 1 ns which is of the same order as the length of the proton bunch and well beyond the acceptable range.

The stability in time of the signal transmission can be significantly improved by active compensation. Part of a signal transmitted from point A to point B (Fig. 6, left) is sent back to the point A and

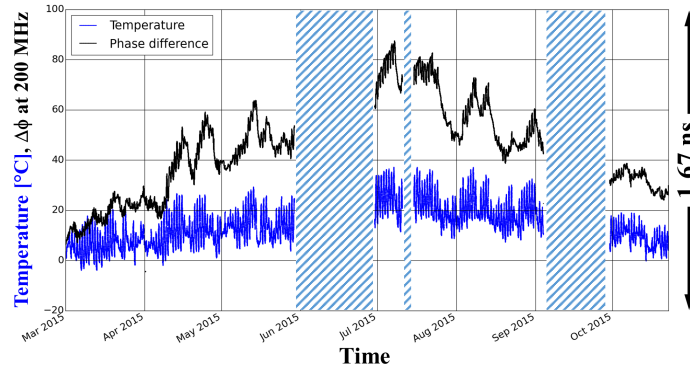


Fig. 5: Drift of a 6.3 km long optical fibre, from the longitudinal beam control system of the CERN SPS to the AWAKE experiment and back [8]. The large fraction of the fibres is installed underground and the temperature may therefore vary along the fibres.

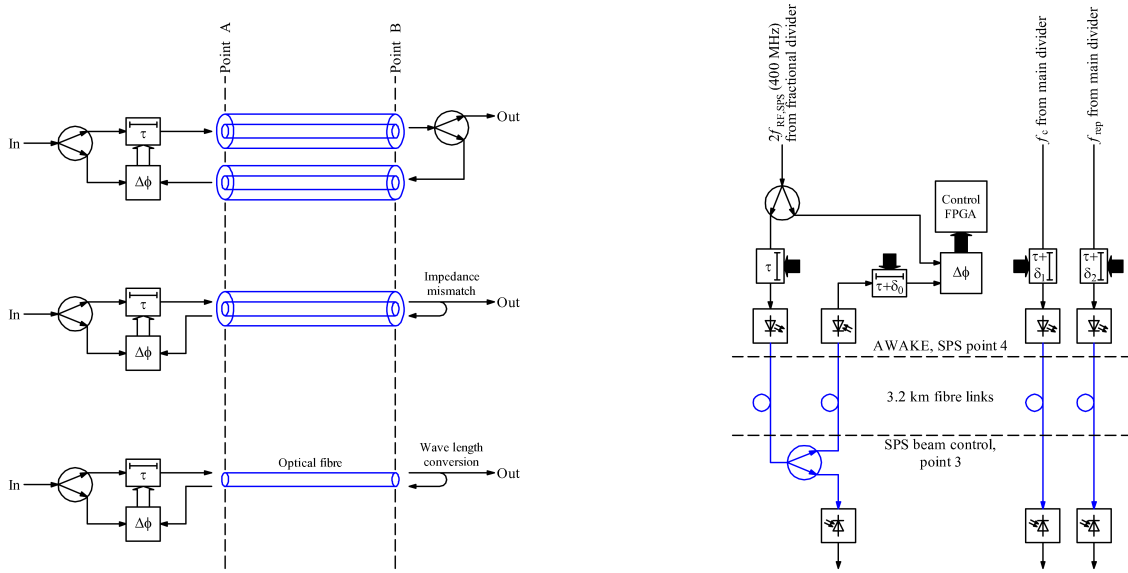


Fig. 6: Principle configurations for active link delay stabilization (left) and set-up to compensate the delay of a link for the AWAKE experiment at CERN between (right). The length of the optical fibres is about 3.2 km [9].

compared there in phase to the source signal. In the most simple case the return signal is split at the destination point and part of it is transmitted back. Such a scheme assumes, however, that the behaviour of both transmissions is identical. This may be difficult to achieve, especially for coaxial cables.

Using the same transmission medium to return part of the signal removes that constraint (Fig. 6, left middle). For a coaxial cable an intended impedance mismatch at the end of the line (point B) causes a reflection travelling back to point A. A directional coupler (not shown) extracts the reflected signal before comparing it in phase with the source signal. The directivity of the directional coupler may limit the achievable performance.

Next to their inherently smaller thermal coefficient of delay, optical fibres also allow to transmit light at several wavelengths simultaneously (Fig. 6, left bottom). The return path can therefore use the same fibre, but at a different wavelength. This removes the need to split forward and reflected waves. To further improve the stability, parts of the link compensation hardware can be implemented optically, e.g., using an optical phase discriminator.

Fig. 6 (right) shows an overview diagram of the optical link for the synchronization of proton bunches from the SPS to the AWAKE experiment at CERN. Next to the compensated transmission of an RF signal at 400.8 MHz, two more signals are sent. Both of them are only required to start counters at a specific period of the RF signal and no particular precision is needed. Their delay simply tracks the one of the 400.8 MHz link to keep all three signals approximately in phase at the arrival in the SPS. Although the configuration with separate optical fibres for forward and return paths stabilizes the delay to the order of 1 ps, the configuration according to Fig. 6 (left bottom) will further reduce the drift.

To obtain even higher stability, the phase measurement and the compensation delay can be implemented as optical components. Ultimately, the phase comparison is performed at a high harmonic of ultra-short laser pulses (5 THz) or directly at the frequency of the light (200 . . . 1000 THz) [1, 10, 11].

2.3 Synchronous frequency dividers

The most common technique to generate a lower frequency from a higher one are frequency dividers. A frequency divider by n , the division ratio, is an electronic counter which counts up to n with every period of the signals at its input. It then generates a pulse at its output and resets itself. Frequency counters exist in many variants, counting up or down, with and without preload, etc. However, independent of their implementation, the counting value of two independent dividers is not necessarily the same.

Fig. 7 illustrates the indeterministic behaviour of two frequency dividers. The circuit on the left

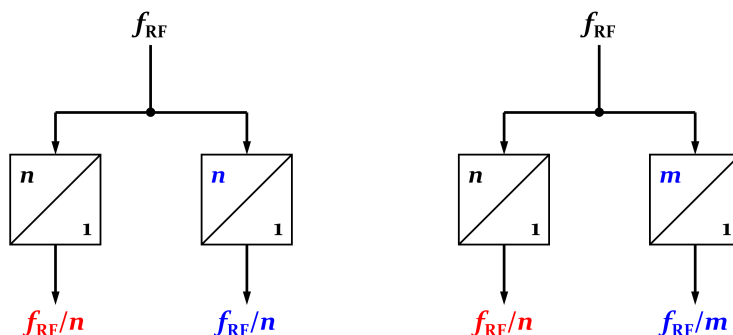


Fig. 7: Configuration of two frequency dividers counting the same input signal. The undefined initial counting state of the dividers results in indeterministic behaviour of the set-up. Both output signals f_{RF}/n (left) may not be identical. The output signals of the circuit dividing by n and m (right) change their relative output phase according to the initial phase.

divides the same RF signal twice by n . However, keeping in mind that the initial condition is not defined when powering the circuit on, the output phase of both dividers can differ by multiples of $2\pi/n$. The circuit on the right (Fig. 7) can even have up to $n \cdot m$ different output phases. Multiple dividers without reset are a common pitfall in synchronization systems. They work correctly until one of the divider misses one or multiple counts with respect the other divider and the relative of the output signals changes.

Two options to force a deterministic behaviour are sketched in Fig. 8. The output of one the two dividers (master, left) is used to reset the second one. This assures that the slave divider starts counting at a well-defined counting state of the master divider. The output signals of both will remain at a fixed phase relationship until one of the dividers misses one clock pulse or counts, e.g., an additional glitch. If a programmable phase shift in units of input clock cycles between both output signals is required (e.g., Sec. 5.2), the circuit shown in Fig. 8 can be employed. The counter value of the first divider is added to an offset by a modulo n counter. This counter wraps around when reaching the programmed division ratio.

In circular accelerators all beam synchronous signals periodic with the revolution period of the

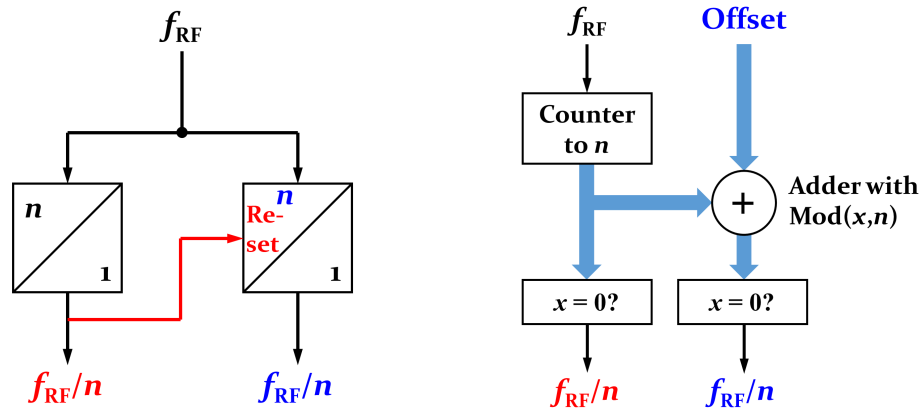


Fig. 8: Configurations to force an unambiguous phase relationship at the output of two dividers. One of the two divider becomes the phase reference (left) and its output resets the second, slave divider. A modulo n adder with a programmable offset (right) can be used to generate a phase offset between both outputs.

circulating beam and dividers are usually reset with a master revolution frequency signal. For the beam transfer between circular accelerators a fiducial or common frequency is chosen with respect to which the whole transfer process is periodic (Sec. 4.1).

2.4 Phase detectors

Measuring and correcting frequency and phase differences between RF signals is important to synchronize beams in different accelerators in preparation of the transfer. The phases of these signals represent the relative azimuthal positions and revolution frequencies of beams in circular accelerators.

Frequency, $\omega = 2\pi f$, and phase, ϕ are actually equivalent, since

$$\omega = \frac{d\phi}{dt} \Leftrightarrow \phi = \int \omega dt. \quad (3)$$

Phase is a relative quantity and phase detectors, also called discriminators, always measure the phase difference between two signals. The Eqs. (3) can also be applied to phase and frequency differences $\Delta\omega = d(\Delta\phi)/dt$. Two special cases are very common in synchronization systems. Firstly, the phase difference of two signals at the same frequency should be detected, e.g., to determine phase between bunches of a beam and the accelerating RF signal. In this case the phase difference is constant with time. Secondly, the frequencies of two signals, e.g., circulating beams in two rings of a collider, are constant, but slightly different. Following Eq. (3) the phase then changes linearly. The latter example is plotted in Fig. 9. However, even an ideal phase discriminator cannot distinguish between a phase difference $\Delta\phi$ and $\Delta\phi + n \cdot 2\pi$. The measured phase difference will hence not just accumulate to infinity, but will wrap around within the range of the phase discriminator. The result is, for the case of two signals with a constant frequency difference, a sawtooth-like phase (Fig. 9).

The most simple phase detector is a frequency mixer, a device which multiplies two signals. This can be easily shown for two sinusoidal at given frequencies ω_n and phases ϕ_n . The product

$$\sin(\omega_1 t + \phi_1) \sin(\omega_2 t + \phi_2) = \frac{1}{2} \{ \cos [(\omega_1 - \omega_2)t + (\phi_1 - \phi_2)] - \cos [(\omega_1 + \omega_2)t + (\phi_1 + \phi_2)] \} \quad (4)$$

can be expressed as a sum of two components at the frequencies $\omega_1 - \omega_2$ and $\omega_1 + \omega_2$. The first component contains the wanted phase difference $\phi_1 - \phi_2$. To extract it, the output signal of the mixer is low-pass filtered to remove the higher frequency component. For the two signals at the same frequency, the phase difference is constant and the low frequency component in Eq. (4) hence becomes just $1/2 \cos(\phi_1 - \phi_2)$.

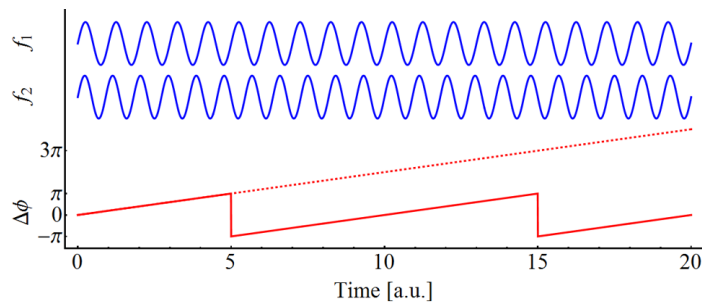


Fig. 9: Phase difference of two signals with slightly different frequency. The phase difference is a linear function with time (red dotted line), but wraps around when measured with a phase detector.

Arbitrarily subtracting a constant phase of $\pi/2$, keeping in mind that the phase detection is a relative measurement, results in a phase dependency proportional to $\sin(\phi_1 - \phi_2)$, which can be approximated to $\Delta\phi = \phi_1 - \phi_2$ for $\Delta\phi \ll 1$. In the given range of phase differences, the frequency mixer will hence indicate the instantaneous phase difference between both inputs (Fig. 10). Table 1 gives a list of

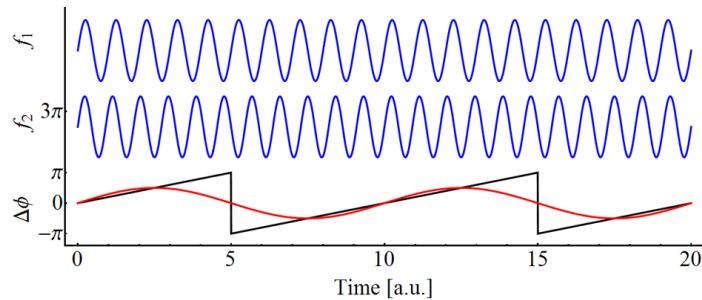


Fig. 10: Phase difference of two signals with slightly different frequency as in Fig. 9. A mixing phase detector only resolves the phase within a small range.

common phase detectors including their basic properties [12, 13]. Phase detectors with full 2π coverage

Table 2: Common phase detector types with range and behaviour.

Type	Range	Behaviour	Reference
Mixer, analogue 4 quadrant multiplier	π	Sinusoidal: $s_{\text{out}} \propto \cos \phi$	[14, 15]
Exclusive OR gate	π	Linear: $s_{\text{out}} \propto \phi - 3\pi/2$, or $s_{\text{out}} \propto -\phi + \pi$	[16]
Sample and hold	π	Sinusoidal: $s_{\text{out}} \propto \sin \phi$	[17]
Flip-flop phase detector	π	Linear: $s_{\text{out}} \propto \phi - \pi$	[12]
Tri-state double flip-flop	2π	Linear: $s_{\text{out}} \propto \phi$	[18]
COordinate Rotation DIgital Computer CORDIC	2π	Linear: $s_{\text{out}} \propto \phi$	[19]
Sagnac loop with optical modulator	$< \pi$	Sinusoidal: $s_{\text{out}} \propto \sin \phi$ (clipped)	[20]

are preferred whenever. They avoid the $\pm\pi$ ambiguity which may, e.g., cause a loop to lock onto an unstable phase.

In terms of absolute precision in time, a phase measurement at a frequency as high as possible is preferable since any error in time is inversely proportional to the frequency, $\Delta\tau = \Delta\phi/(2\pi f)$. However, increasing in frequency may introduce ambiguity. A train of bunches, a so-called batch, spaced by $1/f_{\text{RF}}$ with $f_{\text{RF}} = hf_{\text{rev}}$ can have the same phase every period of the RF frequency. Measuring the phase of the same batch at the revolution frequency defines one unique position of the complete batch per turn.

2.5 Phase-locked loops

A phase-locked loop (PLL) allows to keep two RF or beam signals at a well defined phase relationship. It is also a standard technique to multiply the frequency of a signal, like an inverse frequency divider. The basic building blocks of the PLL are phase discriminator, loop filter and voltage controlled oscillator (VCO) as sketched in Fig. 11. A divider may be added in case the two frequencies to be locked

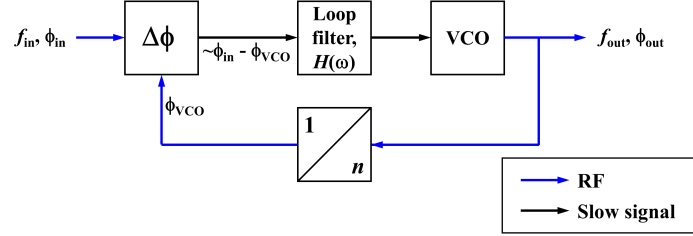


Fig. 11: Typical PLL set-up to synchronize RF signals or to multiply them in frequency.

together are not identical, but in an integer ratio. The input signal, characterised by its frequency, f_{in} , and phase, ϕ_{in} , is compared with the signal from the VCO whose frequency can be controlled closely around $n f_{in}$. The phase difference, a low bandwidth signal proportional to $\phi_{in} - \phi_{VCO}$, is passed through a loop filter which drives the VCO. This closes the loop.

The frequency of the VCO, f_{out} , is hence locked to f_{in} according to $f_{out} = n f_{in}$. At the same time the phase relationship between ϕ_{in} and ϕ_{out}/n is fixed. It is worth noting that the divider does not need to be synchronized as described in Sec. 2.3. The phase comparison is performed with the output signal of the divider with respect to which the counting state is unambiguously defined. The derivation of the transfer function of the PLL is detailed in [12, 21].

Next to its application as a frequency multiplier, the PLL is also used to regenerate signals from a circulating particle beam. In the context of synchronisation systems, this so-called beam phase loop (Sec. 5.1) locks an RF signal to the beam, which allows to derive beam synchronous signals.

3 Longitudinal beam dynamics

The energy gain per turn, ΔE_{turn} , of a particle with the charge, q , in a synchrotron is given by the effective voltage, $V(\phi) = V \sin \phi$, in the accelerating RF cavity at moment of the passage of the particle such that

$$\Delta E_{turn} = qV \sin \phi. \quad (5)$$

To keep the particle on the central orbit, this energy gain must match the energy gain per turn due to the changing magnetic field, $B(t)$,

$$\Delta E_{turn} = 2\pi q \rho R \frac{d}{dt} B(t) = 2\pi q \rho R \dot{B}. \quad (6)$$

The average radius of the accelerator is described by R and its magnetic bending radius by ρ . The combination of Eqs (5) and (6) defines the stable phase

$$\sin \phi_0 = \frac{qV}{2\pi q \rho R \dot{B}}.$$

For a particle with a phase offset, $\Delta \phi$, with respect to the synchronous particle the energy offset can be written as

$$\frac{d}{dt} \Delta E = qV \frac{\omega_{rev}}{2\pi} [\sin(\phi_0 + \Delta \phi) - \sin \phi_0]. \quad (7)$$

The relationship between a frequency and momentum offset is called phase slip factor and defined as¹

$$\eta = \frac{\Delta\omega/\omega}{\Delta p/p} = \frac{1}{\gamma^2} - \alpha_c = \frac{1}{\gamma^2} - \frac{1}{\gamma_{tr}^2}, \quad (8)$$

with the momentum compaction factor $\alpha_c = (\Delta R/R)/(\Delta p/p) = 1/\gamma_{tr}^2$.

Replacing $\Delta p/p = 1/\beta^2 \Delta E/E$ and using [22] $d(\Delta\phi)/dt = -h\Delta\omega$ results in [23]

$$\frac{d}{dt}\Delta\phi = -h\omega_{rev}\frac{\eta}{E\beta^2}\Delta E = -\frac{h\eta}{pR}\Delta E. \quad (9)$$

The ratio between RF and revolution frequency is called harmonic number, $h = \omega/\omega_{rev}$.

Inserting Eq. (7) in the derivative of Eq. (9) results in the equation of motion of a particle in phase

$$\frac{d^2}{dt^2}\Delta\phi + \frac{h\eta\omega_{rev}qV}{2\pi pR} [\sin(\phi_0 + \Delta\phi) - \sin\phi_0] = 0. \quad (10)$$

For small deviations from the synchronous particle the non-linear terms can be approximated according to

$$\sin(\phi_0 + \Delta\phi) - \sin\phi_0 \simeq \cos\phi_0 \Delta\phi$$

and Eq. (10) becomes

$$\frac{d^2}{dt^2}\Delta\phi + \omega_s^2\Delta\phi = 0 \quad \text{with} \quad \omega_s^2 = \frac{h\eta\omega_{rev}qV}{2\pi pR} \cos\phi_0. \quad (11)$$

This is the well known equation of a harmonic oscillator and the frequency of the longitudinal oscillations, ω_s , is called synchrotron frequency.

As will be shown in Sec. 6.5, Eqs. (7) and (9) also define the aspect ratio of the bunch distribution important for the longitudinal matching.

4 Bunch-to-bucket transfer between circular accelerators

For the transfer of bunched beams, the particle distribution from the sending accelerator should be placed in time and energy into the centre of a bucket, the stable region in time-energy phase space (Fig. 12). This requires alignment of the energy of both accelerators, the so-called energy matching, as well as

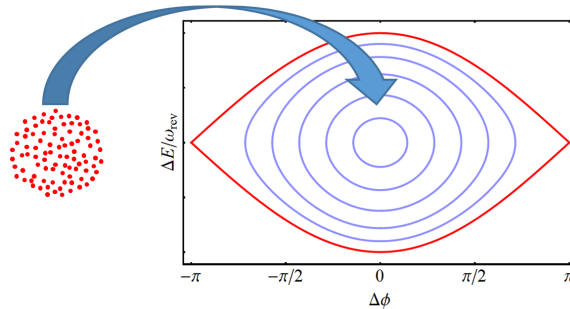


Fig. 12: The bunch-to-bucket transfer places the particle distribution from the sending accelerator into ideally matched RF buckets in the receiving one.

the phase alignment of the RF buckets. A single bunch or a train of bunches can be injected into any bucket, as long as the receiving accelerator has no beam yet and the bunch train fits in terms of length. However, for multiple transfers the bucket number must be carefully controlled to avoid over-injecting

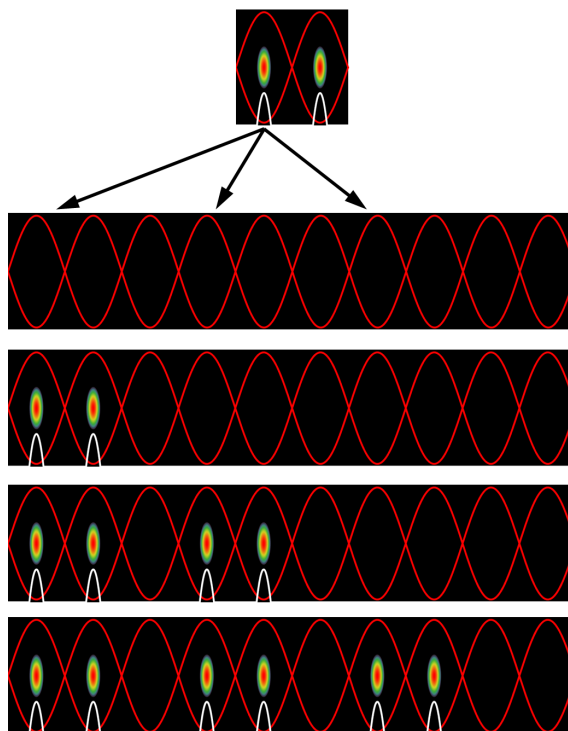


Fig. 13: Longitudinal stacking by bunch-to-bucket transfer of pairs of bunches.

unintentionally into a bucket which is already occupied by a bunch. In Fig. 13 the three injections of two bunches are identical with the exception of the bucket number in the receiving accelerator. The beam structure of filled and empty buckets in an accelerator is referred to as filling pattern.

For the following considerations a synchronized bunch-to-bucket transfer between two circular accelerators is assumed.

4.1 Fundamental periodicity

Before the beam transfer between two circular accelerators, their revolution periods, $T_{\text{rev},1}$ and $T_{\text{rev},2}$, must be synchronized. Though rather common, an integer ratio of revolution periods is generally not required. The ratio can also be fractional such that

$$T_{\text{rev},2} = \frac{n_1}{n_2} T_{\text{rev},1} \quad \leftrightarrow \quad n_2 T_{\text{rev},2} = n_1 T_{\text{rev},1} \equiv T_{\text{common}} = T_{\text{fiducial}}$$

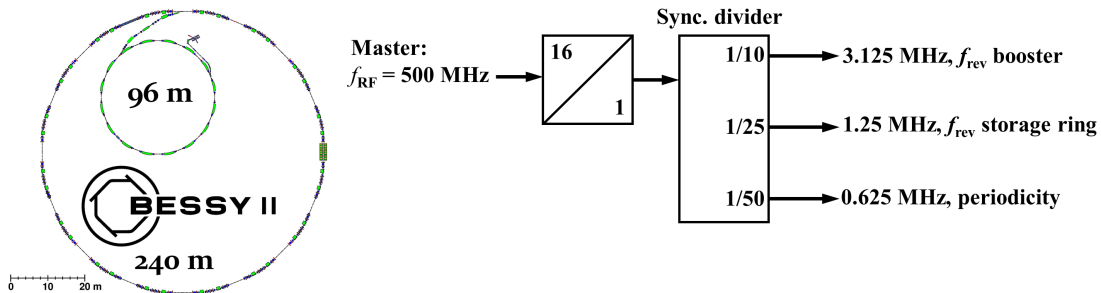
The time period with which the whole system of both beams repeats is often referred to as super-period, common or fiducial period. Hence a beam transfer can take place under the same conditions every n_1 turns of the accelerator with a revolution period of $T_{\text{rev},1}$ which is identical to n_2 turns of a beam at $T_{\text{rev},2}$. Integer revolution period ratios simplify the transfer which can then take place at any turn of the larger of the two accelerators.

Table 3 summarizes the revolution frequency ratios for some accelerator facilities. An example for two electron synchrotrons with a non-integer revolution frequency ratio are booster and storage ring at BESSY II as illustrated in Fig. 14. All signals are directly derived from a reference generator at close to $f_{\text{RF}} = 500$ MHz, the main RF frequency of both booster and storage ring. Following a frequency division by 16, the resulting signal at 31.3 MHz is then synchronously divided by 10, 25 and 50 to obtain the revolution frequency of booster and storage ring, as well as the frequency of the super-period.

¹The phase slip factor is sometimes defined with the opposite sign, e.g. [24].

Table 3: Revolution frequency ratios of selected accelerator facilities.

BESSY Booster	BESSY SR	2/5	Fixed frequency
SLS Booster	SLS SR	15/16	Fixed frequency
J-PARC RCS	J-PARC MR	2/9	Profit from ratio for bucket selection
GSI SIS12/18	GSI ESR	2/1	
CERN PS Booster	CERN PS	1/4	
CERN PS	CERN SPS	1/11	
CERN PS	CERN AD	3/1	Particle type and energy change at transfer
CERN SPS	LHC	7/27	$f_{\text{common}} = 1/T_{\text{common}}$ as low 1.6 kHz

**Fig. 14:** Generation of beam synchronous frequencies at the BESSY facility (courtesy of BESSY).

The periodicity is illustrated in Fig. 15 for the example of the BESSY II facility with a revolution frequency ratio of 2/5. With every half turn of the bunch in the booster synchrotron the bunch in the storage ring advances by $1/2 \cdot 2/5 = 1/10$ th of a turn. As expected, the azimuthal position of the bunches is identical every 5 turns of the booster, equivalent to every 2 turns in the storage ring.

4.2 Beam synchronous triggers

As mentioned above several devices need to be triggered shortly before, during or after the beam transfer, in particular fast kicker magnets and fast beam instrumentation. These beam synchronous triggers can be generated by chains of counters counting beam synchronous clocks. Such a cascade of counters is sketched in Fig. 16. The transfer process is launched by the master start which does not need be to synchronous to anything. It is just a time marker to indicate the upcoming transfer. The first counter in the chain counts the super-period. The value to which is counts is not relevant, but the fact that the trigger #1 is generated based on the super-period clock, i.e., the fundamental periodicity of the transfer. Since all clocks are derived from a common reference, the super-period clock is synchronous with the revolution and RF clocks. One can hence simply chain a counter on the revolution frequency #2 and a further one on the RF frequency. This allows to generate an unambiguous trigger #3 anywhere in time with a granularity of the revolution or RF period and corresponds to the bucket number. This scheme allows to select a specific turn and bucket number.

For a beam transfer between two accelerators, such triggers must be generated on the sending and on the receiving side both of which may, in large facilities, be several kilometres apart from each other. This is easily achieved by adding parallel branches to the timing cascade (Fig. 17). As the counters in sending and receiving accelerator are started with a common trigger synchronous to the super-period clock and, since all clocks (super-period and revolution frequency clocks) have a fixed phase relationship, the delay between the triggers #2 and #3 in Fig. 17 is reproducible. Again counters using the RF clock allow the adjustment of bucket numbers.

Thanks to the practically constant revolution frequencies of electrons, the basic ingredients to generate all beam synchronous triggers are complete for the transfer of beams between circular lep-

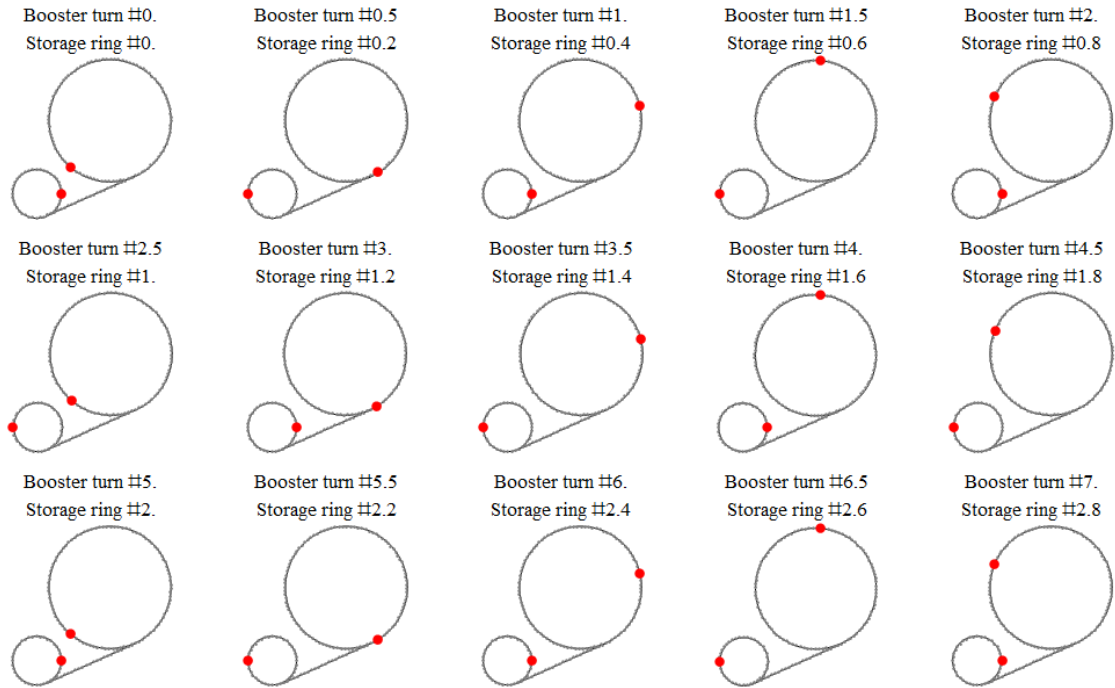


Fig. 15: Bird's eye view of the facility Fig. 14, with a revolution frequency ratio of $2/5$. Snapshots are taken every half turn of the booster synchrotron. Note that in BESSY the beams in both accelerators circulate clockwise.

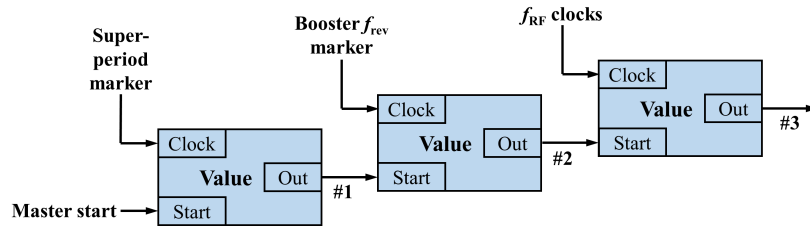


Fig. 16: Generation of beam synchronous triggers.

ton accelerators. Additionally, due to the strong synchrotron radiation damping at electron energies in the GeV regime, the precision in time is usually not very demanding. As long as the bunch is injected into the correct bucket it will be forced into the centre of the bucket by synchrotron radiation.

All signals can be derived from a common, fixed-frequency master oscillator which makes the entire transfer process fully deterministic in lepton accelerators. Starting from an event triggering the transfer, all beam synchronous signals for kicker magnets or fast diagnostics to monitor the transfer, all timing triggers are derived by counting the RF master clock or a one of its sub-multiples. Everything is predictable from the beginning, which significantly simplifies the synchronisation and timing system for the beam transfer compared to the one of hadron accelerators.

5 Transfer between hadron accelerators

Due to the slower velocity of hadrons, the revolution frequency changes during acceleration by a considerable amount. Especially in low energy hadron synchrotrons it may sweep by several octaves. In the Extra Low ENergy Antiproton (ELENA) ring at CERN it changes by almost one order of magnitude, whereas the relative particle velocity in the LHC only increases by a few 10^{-6} during acceleration.

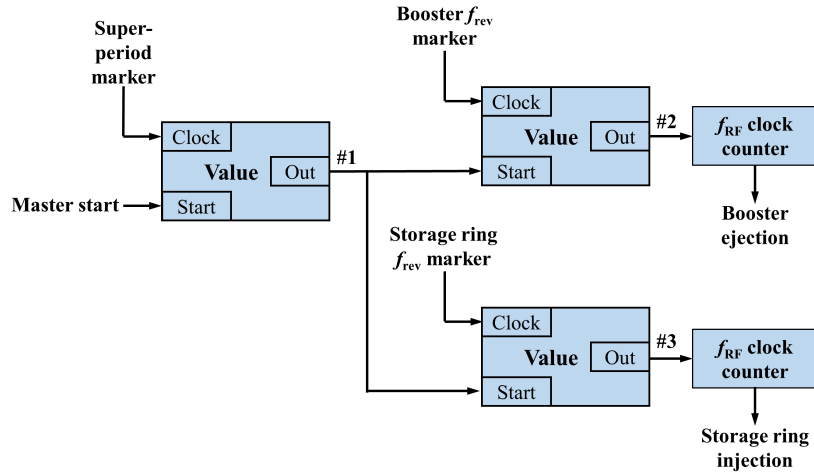


Fig. 17: Generation of multiple beam synchronous triggers.

With the revolution frequency sweep, also all counters generating beam synchronous timings for kickers and beam instrumentation must be supplied with sweeping clocks. The delay of cables and electronics, τ , leads to a frequency dependent phase according to $\Delta\phi = 2\pi h f_{\text{rev}} \tau$ for any signal at the h th harmonic of the revolution frequency. The exact revolution frequency is moreover derived from the beam, via the beam phase loop.

The absence of synchrotron radiation damping also poses more stringent requirements on the transfer. It is not sufficient to place the bunch into the correct bucket and let it move to the exact energy and phase of the bucket in the receiving accelerator. The injected hadron bunch must be placed into the centre of the bucket in terms of phase and energy instead (Fig. 12). Additionally, the aspect ratio of the injected bunch, the ratio between bunch length and energy spread, must correspond to the aspect ratio of the bucket in the receiving accelerator. This can be achieved by longitudinal matching (Sec. 6.5).

The harmonic number during the acceleration may be changed with so-called RF manipulations. In the presence of two RF harmonics simultaneously a beating pattern of the effective RF voltage depending on the azimuth position of the bunches is generated. This splits the behaviour for different bunches, thus requiring careful counting of bucket numbers.

5.1 Beam phase loop

Due to the absence of synchrotron radiation damping, the bunch in a hadron accelerator does not match itself to the bucket. Any error in phase or energy will cause longitudinal oscillations which, due to the non-linearity of these synchrotron oscillations, lead to uncontrolled growth of the spread of the particle distribution.

In hadron synchrotrons the beam itself is therefore used as a reference for the phase of the RF voltage which keeps it bunched and accelerates it. This is an application of the PLL introduced in Sec. 2.5. Figure 18 shows a simplified diagram of a PLL in the configuration of a beam phase loop. The beam phase is compared with the phase from a probe of the voltage in the accelerating cavity. This phase difference gives the longitudinal position of the particle bunch with respect to the RF bucket. As the reference phase of the bucket intentionally moves during acceleration, the synchronous phase, ϕ_s , must be subtracted from the measured phase difference between beam and acceleration RF signals. This bunch-to-bucket phase error then pilots, via a loop filter, the frequency correction of a precision VCO generating the signal at $f_{\text{RF}} = h f_{\text{rev}}$ driving the power amplifier. The configuration of the PLL is hence the same as sketched in Fig. 11, but with the beam replacing the input signal.

To minimize the errors to be corrected by the loop, the VCO is implemented as an oscillator

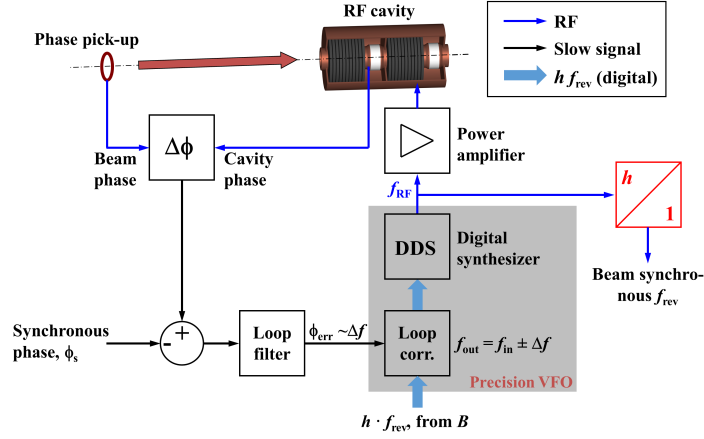


Fig. 18: Typical overview diagram of a beam phase loop.

which can only be tuned in a small range around the expected revolution frequency of the beam. This expected revolution frequency can be derived from the knowledge of the magnetic bending field defining the energy of the accelerator.

Compared to the standard electronic phase-locked loop (Sec. 2.5) the beam behaviour now contributes to the transfer function of the beam phase loop. It can be included by calculating the response of the beam in phase to a change of frequency driven by the RF system.

As shown in Sec. 3 the energy offset change for small deviations in $\Delta\phi$ with respect to the synchronous phase can be approximated, and the equations of motion become

$$\frac{d}{dt}\Delta E = qV \frac{\omega_{\text{rev}}}{2\pi} \cos \phi_0 \Delta\phi \quad (12)$$

$$\frac{d}{dt}\Delta\phi = -\frac{h\eta}{pR}\Delta E + \delta\omega_{\text{RF}}. \quad (13)$$

A small frequency modulation by the RF system contributes as a perturbation term, $\delta\omega_{\text{RF}}$, and is added in Eq. (13) to the phase change from the energy offset [25].

To extract the longitudinal beam transfer function in frequency domain, the equations can then be solved by an ansatz $\Delta\phi(t) = \Delta\phi e^{i\omega t}$ and $\Delta E(t) = \Delta E e^{i\omega t}$. The equations of motion then simplify to

$$i\omega\Delta E = qV \frac{\omega_{\text{rev}}}{2\pi} \cos \phi_0 \Delta\phi$$

$$i\omega\Delta\phi = -\frac{h\eta}{pR}\Delta E + \delta\omega_{\text{RF}}$$

in frequency domain, which can be solved to

$$\Delta\phi = \frac{i\omega}{\omega_s^2 - \omega^2} \delta\omega_{\text{RF}}. \quad (14)$$

This is the response of the beam in phase to a perturbation of the driving RF frequency. Replacing $s = i\omega$, the beam transfer function hence becomes

$$H(s) = \frac{\Delta\phi}{\delta\omega_{\text{RF}}} = \frac{s}{\omega_s^2 + s^2}. \quad (15)$$

Dividing the RF frequency from the precision VCO (Fig. 18, divider marked in red) by the harmonic number, h , results in a revolution frequency signal with fixed relationship with respect to the beam and maintained by the beam phase loop. It can be used to clock counters generating beam synchronous triggers, and it represents the longitudinal beam position for a synchronization loop discussed below.

5.2 Beam synchronous revolution frequency

Deriving a beam synchronous revolution frequency by division (Fig. 18) from an RF signal locked to the beam introduces the ambiguity of the phase depending on the counting state of the divider (Sec. 2.3). The most common approach to avoid this ambiguity is counting RF cycles correctly right from the beginning. With the first injection the beam is already transferred with a reproducible delay with respect to the output of the revolution frequency divider.

Moving the beam in time with respect to the beam synchronous revolution frequency can be easily achieved by simply inserting a delay into the branch to the sending accelerator (Fig. 19, left). Since

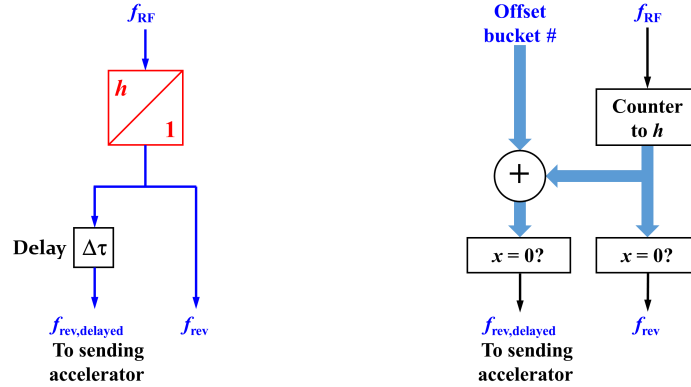


Fig. 19: Set-ups to achieve a reproducible phase relationship between the beam synchronous revolution frequency and the injected beam. Technically the delay (left) is mostly implemented with counters allowing to comfortably adjust the arrival time of the incoming beam in units of RF buckets.

the delayed revolution frequency, $f_{\text{rev,delayed}}$, to the upstream accelerator and the internal revolution frequency, f_{rev} , are derived from the same source, after the frequency division, both have an unambiguous phase relationship by definition.

Adjustable delays are technically difficult to realize, in particular for large accelerators, where one turn can take several tens of microseconds. The delayed revolution frequency can be generated by an offset counter (Fig. 19, right) more easily, as introduced in Sec. 2.3. The offset is programmed in units of input clock cycles of the counter, which is usually the bucket number when counting f_{RF} .

For multiple injections, the bucket number offset is simply changed in between transfers, such that multiple injections with a programmable filling pattern can be achieved. The beam synchronous revolution frequency will always have a reproducible delay or phase with respect to the circulating beam. It therefore indicates the longitudinal position of the beam.

5.3 Bucket numbering

Keeping track of the position of occupied and empty RF buckets is essential to prepare an intended filling pattern in the case of multiple injections. A newly injected bunch should not be placed in time into an already occupied bucket, as the circulating bunch would be removed by the injection kicker and replaced by the incoming one.

Measuring whether a bucket is empty or occupied by a bunch must not be necessary in the framework of the beam transfer process. Using beam signals to derive triggers for the beam transfer is not appropriate since a bunch may be missing [26] or may have an intensity or profile which would now allow a correct detection.

Bunches are always injected with a well defined delay with respect to a beam synchronous revolution frequency. The beam synchronous revolution frequency itself has a reproducible delay with respect

to the circulating beam since every injection is performed using it as a reference for the longitudinal beam position. Hence, knowing the sequence of injected bunches, allows to keep track of the filling pattern in a synchrotron.

In an accelerator with a single harmonic RF system, and neglecting any intensity effects, all RF buckets are equal. This changes when applying two or more RF harmonics simultaneously. The greatest common divider of all involved RF harmonics defines the frequency with which the sum RF voltage is periodic. In the extreme case, when the harmonic numbers have no common divider other than one, the total RF voltage is only periodic with the revolution frequency. Consequently, the size and form of all RF buckets becomes different.

The longitudinal phase space for such a case is shown in Fig. 20, where the RF voltage is the same at two harmonics, $h = 9$ and $h = 10$ [27]. This bucket configuration is present in the middle of a

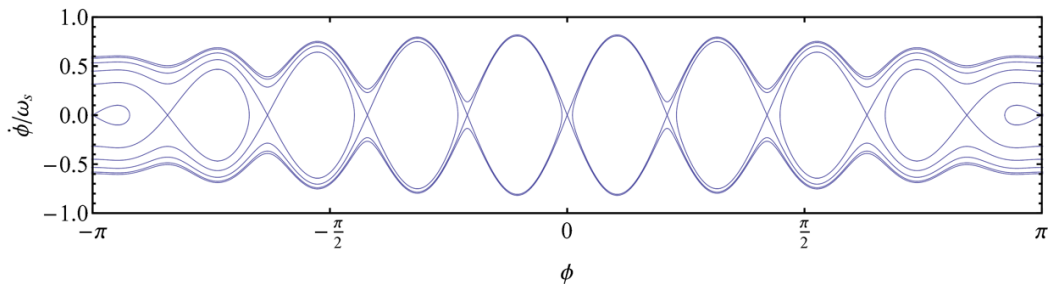


Fig. 20: Normalized longitudinal phase space for a double harmonic RF system with equal voltage at both harmonics, $h = 9$ and $h = 10$.

so-called batch compression process in the PS at CERN. The spacing between bunches can be reduced by incrementally moving to a larger RF harmonic. This happens at the cost of introducing an additional RF bucket at an azimuth which should not be occupied by particles (Fig. 20, at $\phi = \pm\pi$).

Due to the periodicity of the RF voltage with the revolution frequency, there are nine possibilities of injecting eight bunches into the nine buckets (Fig. 21, left). Only one of them (right) keeps the empty bucket at the location where the additional bucket is introduced during the $h = 9$ to $h = 10$ handover. This example at the beam transfer between PS Booster (PSB) and PS illustrates the importance of bucket numbering.

In accelerators performing RF manipulations like the PS at CERN, the number of bunches may change during the acceleration cycle as the one shown in Fig. 21. Depending on the type of manipulation, even the position of the first bunch with respect to the beam synchronous revolution frequency changes. Therefore, prior to ejection, the bucket numbering must be rearranged to realign, e.g., the position of the first bunch with respect a phase reference given by the receiving synchrotron.

Renumbering the buckets for extraction practically means to shift signal phases such that the RF synchronization process will move the beam to the intended, reproducible phase with respect to the external reference marker from the receiving accelerator. As will be shown in Sec. 6.3, a reference revolution frequency, marking the expected position of the beam after synchronization, is compared in phase to the internal beam synchronous revolution frequency. Acting on the phase of either of these two signals moves the relative delay of the marker from the receiving accelerator and the extracted beam.

For the example of the transfer between PS and SPS at CERN, where the SPS as a receiving synchrotron defines the azimuth position of the bunches, it turns out to be technically more easy to move the phase of the reference for the synchronization. The simplified set-up is sketched in Fig. 22. A synchronous frequency divider (Sec. 2.3) generates a signal at the revolution frequency of the PS to serve as a reference for the RF synchronization. It is compared in phase with the beam synchronous revolution frequency. The reset for the divider is generated from the revolution frequency marker from the SPS,

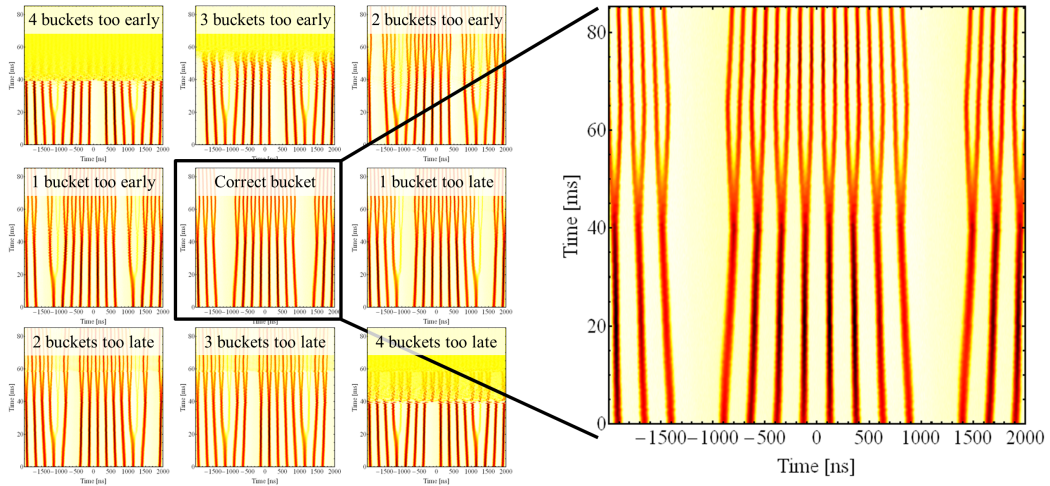


Fig. 21: Measured mountain range plots when injecting eight bunches into $h = 9$ in the PS and moving them from harmonic $h = 9$ to 10 (first 40 ms) and further via $h = 20$ to 21. The RF voltages at $h = 9$ and $h = 10$ are equal at 20 ms after the start of the manipulation and the longitudinal phase space corresponds to the one illustrated in Fig. 20. The azimuth of the incoming bunches is moved with respect to the RF buckets by multiples of $h = 9$ buckets, $n \cdot 2\pi/9$, $n = 0 \dots 8$.

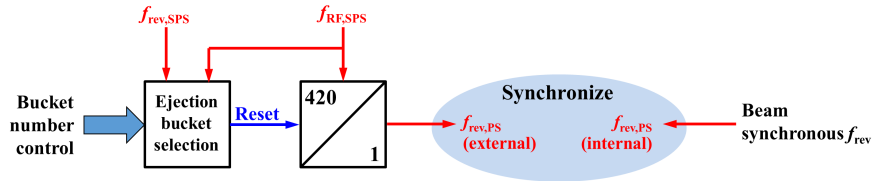


Fig. 22: Simplified diagram of the ejection bucket numbering system between PS and SPS. The reference revolution frequency for the RF synchronization is shifted in phase with respect to the revolution frequency marker from the SPS.

but delayed by a programmable number of RF clocks, again from the SPS. This shifts the reference revolution frequency in programmable steps of SPS buckets, and with it the phase position of the beam in the PS with respect to the revolution frequency marker from the SPS. This mechanism allows to adjust the phase position of the outgoing bunches of the extracted such that the position of the bucket with, e.g., the first bunch is aligned with respect to the expected position, independent of RF manipulation or injection bucket numbering in the PS.

6 Synchronization and transfer

The bunch-to-bucket transfer of beam between circular hadron accelerators usually follows a sequence of energy matching, RF synchronization and further actions directly related to the transfer. These steps are summarized in Tab. 4 in chronological order [28]. The first two steps prepare the bunch-to-bucket transfer. Thereafter the transfer can take place with every cycle of the fundamental periodicity (Sec. 4.1). The remaining steps are all related to the transfer itself, trigger elements required for the extraction and injection bumps, the septa. The last step is the generation of triggers for the ejection and injection elements which guide the beam to the transfer line trajectory at the exit of the sending accelerator and back to the trajectory for the circulating beam in the receiving accelerator.

Table 4: Chronological order of steps relevant to synchronization and timing at beam transfer.

1.	Set bending fields in both accelerators to the same magnetic rigidity Prepare transfer line
2.	RF synchronization of sending or receiving accelerator
→ Ready for transfer	
3.	Start counting clock of fundamental periodicity Trigger bump and septum elements
4.	Start counting f_{rev} clock (sending and receiving accelerator independently) Start counting bucket clock
5.	Fine delays started Ejection and injection kicker triggers
→ Transfer	

6.1 Matching of bending strength

Matching the bending field in both accelerators to the same magnetic rigidity is a first precondition to prepare the beam transfer [29].

To keep charged particles on a circular trajectory, the centripetal force, F_Z , must be compensated by the Lorentz force, F_L . This equality can be written such that the particle properties momentum, p , and charge, q , are separated from the accelerator parameter bending radius, ρ and strength, B :

$$F_Z = F_L \quad \rightarrow \quad \frac{p}{q} = \rho B. \quad (16)$$

As long as the energy, charge state and type of the particle remain unchanged during the transfer, the magnetic rigidity must be the same in sending and receiving accelerator,

$$\rho_1 B_1 = \rho_2 B_2. \quad (17)$$

Exceptions are transfers with particle type change in the line between both accelerators. Anti-protons are produced by conversion on a target between the accelerator for the primary beam and the one collecting the anti-protons from the debris produced at the target. At Fermilab a proton beam at an incident momentum of $p = 120 \text{ GeV}/c$ was producing anti-protons at $8 \text{ GeV}/c$. The Anti-proton Decelerator (AD) at CERN receives anti-protons at a momentum of $p = 3.6 \text{ GeV}/c$ produced by a primary proton beam at $26 \text{ GeV}/c$ from the PS. A different magnetic rigidity is also needed when the charge state changes during beam transfer. In the ion injector chain at CERN charge state $^{208}\text{Pb}^{54+}$ in the Low Energy Ion Ring (LEIR) and PS is stripped to $^{208}\text{Pb}^{82+}$ in the transfer line between PS and SPS. In addition to the change of charge state, the stripping process also causes an average energy loss of the beam. The magnetic rigidities are programmed according to Eq.(16).

6.2 Matching RF frequencies and bunch distance

Besides the bending fields, also the RF frequencies in both accelerators must have a distinct ratio. Assuming that the beam velocity is unchanged during the transfer and using $f_{\text{rev}} = f_{\text{RF}}/h = \beta c/(2\pi R)$, the condition for the ratios of RF frequencies, harmonic numbers and average radii becomes

$$\beta c = 2\pi R_1 f_{\text{rev},1} = 2\pi R_2 f_{\text{rev},2} \quad \rightarrow \quad R_1 \frac{f_{\text{RF},1}}{h_1} = R_2 \frac{f_{\text{RF},2}}{h_2}. \quad (18)$$

A common choice, in particular for most electron accelerators, is to operate sending and receiving accelerator at the same RF frequency, $f_{\text{RF},1} = f_{\text{RF},2}$ (Fig. 23, left) at transfer. The harmonic number simply becomes proportional to the ring circumference, $2\pi R$. Again, Eq. (18) is only valid for fixed velocity

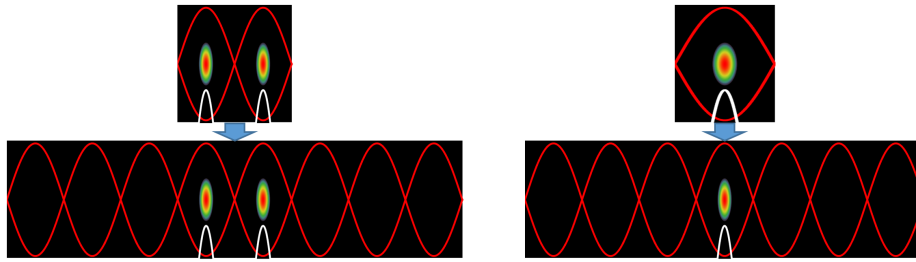


Fig. 23: Bunch-to-bucket transfer with equal (left) and unequal (right) RF frequencies.

during the transfer, which is not the case, e.g., for the production of anti-protons at a target in the transfer line. The velocity factors β_1 and β_2 must be added in the denominators of Eq. (18).

Next to the RF frequencies also the distance between bunches in the sending accelerator must match the distance of the buckets in the receiving one to transfer multiple bunches with a single transfer. An integer ratio of RF frequencies is common in cascades of hadron synchrotrons. At the transfer of protons for the LHC between PS and SPS, the RF frequency in the SPS, $f_{\text{RF,SPS}} = 200.3$ MHz, is five times the principal RF frequency in the PS of about 40.1 MHz, while at transfer to the LHC, the RF frequency in the LHC is twice larger than the one in the SPS. By definition, the PS can hence fill every 5th bucket in the SPS, and the bunches from the SPS can only occupy every second bucket of the LHC. The accelerator chain of PS and SPS consequently transfers one bunch into every 10th bucket of the collider.

Of course the bunch distance is only relevant for the transfer of more than one bunch. This gives more flexibility at the transfer from the PS Booster (PSB) to the PS at CERN. While the PS is four times larger in circumference than the PSB, suggesting that $h_{\text{PS}} = 4h_{\text{PSB}}$, many more combinations of harmonic numbers are possible thanks to the transfer of single bunches, e.g., $h_{\text{PS}}/h_{\text{PSB}} = 7$ or 9.

A further exception is the transfer using multi-harmonic RF systems in one of the accelerators. In the PSB, two bunches at $h_{\text{PSB}} = 2$ with a natural distance for an injection into the PS at $h_{\text{PS}} = 8$, have been pushed further apart to inject them into $h = 7$ buckets in the PS [30].

6.3 RF synchronization

Even with the magnetic rigidity set according to Eq. (16), the beam derived revolution frequencies eventually will not be at their theoretical ratio due to imperfections of bending field strength and length of beam orbit. These errors lead to a slippage of the bunches with respect to the positions of the buckets, which is illustrated in Fig. 24. The bucket positions in the sending accelerator, projected into the receiving one (Fig. 24, grey dots), move in time with respect to the real bucket positions (Fig. 24, purple dots). This phase slippage is caused by the revolution frequencies not being exact integer or rational multiples.

Before starting the RF synchronization to lock the revolution frequencies of two accelerators [31], it must be decided if the sending synchrotron should be synchronized to the receiving one or vice versa.

For a bunch-to-bucket transfer with the sending accelerator as master for the beam transfer, revolution frequency and bucket positions in the receiving adapt to the incoming beam. This is a common choice when the receiving accelerator has no beam before the transfer. An example is the injection of anti-protons into the AD ring at CERN which are generated by an incident proton beam from the PS.

However, for multiple transfers there is little interest in synchronising the receiving accelerator, as every synchronisation process requires to move all bunches to the revolution frequency of the newly incoming beam, perturbing the accumulated bunches more than necessary. Therefore the receiving accelerator is commonly chosen as master whenever it already has beam before the transfer and in particular for the case of multiple transfers. Only the newly injected beam needs to be synchronized and may suf-

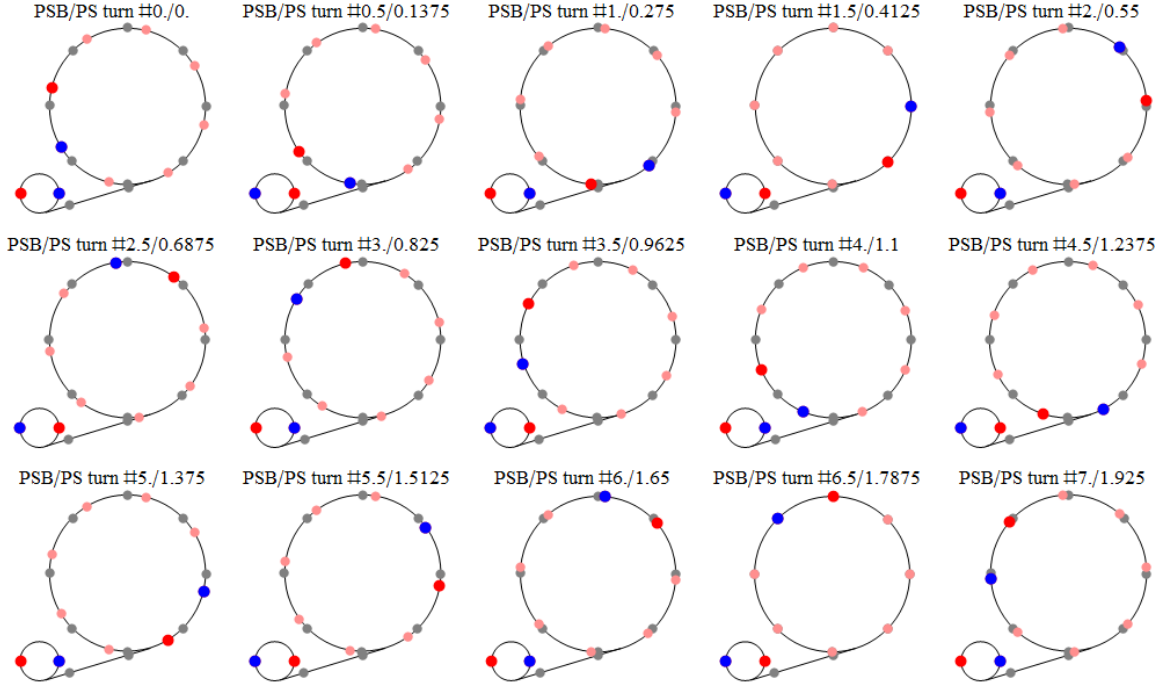


Fig. 24: Bird's eye view of the PSB ($h_{\text{PSB}} = 2$) to PS ($h_{\text{PS}} = 8$) transfer before the RF synchronization. The circulating bunches are indicated by blue and red dots. Empty bucket positions are marked as grey dots in the sending accelerator and purple in the receiving one.

fer once from the synchronization process. Multiple re-synchronizations of the accumulated beam are avoided. It is the most common choice and implemented in, e.g., the injector chain of the LHC. Without loss of generality, the receiving accelerator is considered as the master of the beam transfer in what follows.

Even though the relative phase of beams moves corresponding to revolution frequency errors (Fig. 24) [32], this slippage is usually too slow to just wait until the intended phase relationship is reached for a possible transfer. Firstly, the beam to be synchronized is therefore, at constant bending field, $dB/dt = 0$, slightly accelerated or decelerated to an off-momentum orbit according to Eqs. (8) and (26)

$$\frac{df}{f} = \frac{\gamma_{\text{tr}}^2 - \gamma^2}{\gamma^2 \gamma_{\text{tr}}^2} \frac{dp}{p},$$

which establishes a defined frequency difference between the accelerators. Secondly, the azimuth error is measured to close a synchronization loop when the beam is at the intended azimuthal position.

As introduced in Sec. 2.4, a constant frequency error between to RF signals translates into a linearly changing phase difference (Fig. 25), as measured at the phase detector comparing the reference azimuth and the actual beam azimuth. Once the reference phase position is reached, the synchronization loop closes by acting on the RF frequency of the synchronized accelerator. Azimuth, revolution and RF frequencies are then locked with respect to the external reference.

An example of the phase measurement between reference and actual beam position during the synchronization of the bunches in the SPS prior to their transfer to the LHC [33] is illustrated in Fig. 26, together with the synchronization steps and their effect on the phase of the beam. Following the arrival at the flat-top, the revolution frequency of the SPS is moved to $f_{\text{RF,SPS}} = 27/7 f_{\text{RF,SPS}}$. Both beams in SPS and LHC are then circulating according to the fundamental periodicity Eq. (4.1) such that $T_{\text{common}} = 27T_{\text{rev,SPS}} = 7T_{\text{rev,LHC}}$. The azimuth error of the whole beam in the SPS is measured and a frequency

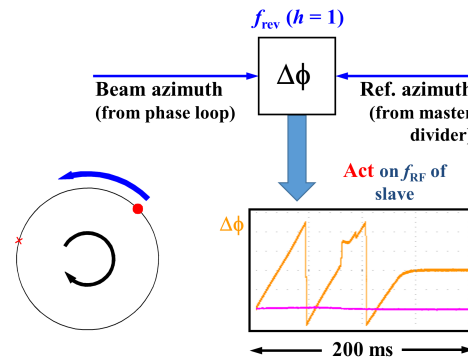


Fig. 25: Synchronization loop to move the beam to an intended azimuthal position.

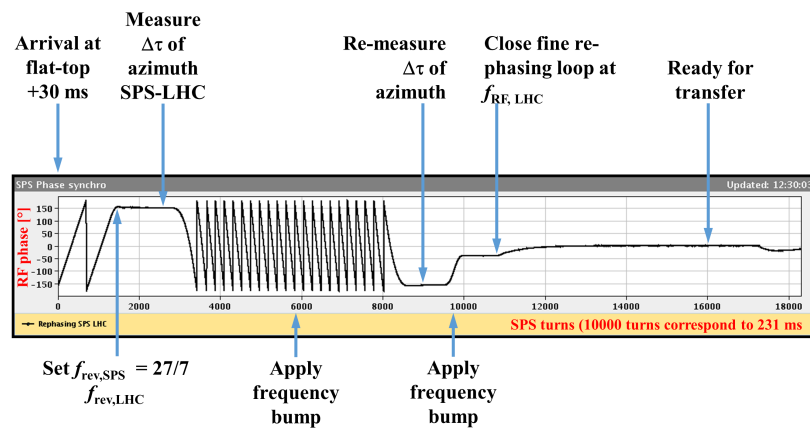


Fig. 26: Phase detector at twice the RF frequency in the SPS during the synchronization before the transfer to the LHC.

bump is generated to move the actual to the reference azimuth. This sequence of measurement and frequency bump repeats until the beam has been moved to the reference azimuth within an accuracy of much better than the azimuth $2\pi/h$ of one RF bucket.

To then precisely align the bunch centres with respect to the position of the bucket centers in the LHC, a synchronisation loop compares the reference RF at about 400.8 MHz from the LHC with twice the RF frequency (about 200.4 MHz) in the SPS and locks them together.

Following this synchronization process, which takes about half a second, the beam in the SPS circulates synchronously and at the correct azimuth position with respect to the beam in the LHC. The transfer process can be launched with every period of the fundamental periodicity.

Putting all relevant parts of the RF synchronization system together, the synchronization chain between outgoing beam and the reference marker signals at which the beam is actually expected, is illustrated in Fig. 27. The beam to be extracted is locked at a reproducible phase relationship with

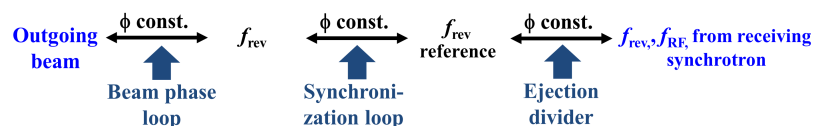


Fig. 27: Synchronization chain from the reference signal of the receiving accelerator to the extracted beam of the sending one.

respect to the beam synchronous revolution frequency, f_{rev} by the beam phase loop (Sec. 5.1). This beam synchronous revolution frequency is itself kept at a constant phase with respect to the external reference revolution frequency by one or several synchronization loops. Finally, the external revolution frequency for the sending synchrotron is generated from the shifted reference RF and revolution frequency signals of the receiving synchrotron, again at a fixed phase relationship. In summary, the beam in the sending accelerator and the reference marker from the receiving one are in a reproducible phase relationship. By shifting its reference signals the receiving synchrotron controls when in time the beam must be delivered by the sending synchrotron. This concept allows complex filling patterns generated under full control of the receiving accelerator. For the sending synchrotron all beam transfers are simply the same.

Once the RF synchronization completed the case of two proton accelerators is exactly identical to the case of two electron accelerators prior to the transfer, with an integer or rational revolution frequency ratio (Fig. 15). The beams are synchronized and can be extracted with every marker of the fundamental periodicity.

6.4 Energy matching

In an ideal synchrotron the beam circulates exactly at the expected revolution frequency, $\Delta f_{\text{rev}} = 0$, on the central orbit, $\Delta R = 0$ and it has the reference momentum, $\Delta p = 0$. A real accelerator has errors on all of these parameters.

6.4.1 General orbit equation and differential relations

According to Eq. (16) a particle on the central orbit (index zero) has a momentum given by

$$p_0 = qB\rho_0. \quad (19)$$

For a particle with a momentum offset, the orbit length is defined via the transverse optics by the momentum compaction factor at constant magnetic field [34]

$$\alpha = \frac{1}{\gamma_{\text{tr}}^2} = \frac{\partial L/L}{\partial p/p} = \frac{\partial R/R}{\partial p/p} = \frac{p}{R} \frac{\partial R}{\partial p}, \quad (20)$$

where $L = 2\pi R$ is the circumference. Integration of Eq. (20) results in

$$\ln R = \alpha \ln p + c_1 \quad \Leftrightarrow \quad R^{1/\alpha} = p e^{c_1/\alpha} = c_2 p \quad \text{with} \quad c_2 = e^{c_1/\alpha}. \quad (21)$$

The variables c_1 and c_2 are arbitrary integration constants.

The latter constant c_2 can be derived by keeping in mind that Eq. (21) must again be fulfilled by the reference particle with a momentum, p_0 , given by Eq. (19), hence

$$R^{1/\alpha} = c_2 p = c_2 qB\rho_0 \Leftrightarrow c_2 = \frac{R_0^{1/\alpha}}{qB\rho_0}.$$

The circumference for the reference particle is $2\pi R_0$. This leads to the generalization of Eq. (19) for a particle at any average radius [34, 35]

$$p = qB\rho_0 \left(\frac{R}{R_0} \right)^{1/\alpha}. \quad (22)$$

Based on this general equation, a set of differential relations can be derived for particles with a small derivation from the reference parameter as summarized in the table below [34].

Variables	Relation	
B, p, R	$\frac{dp}{p} = \gamma_{\text{tr}}^2 \frac{dR}{R} + \frac{dB}{B}$	(23)

f, p, R	$\frac{dp}{p} = \gamma^2 \frac{df}{f} + \gamma^2 \frac{dR}{R}$	(24)
-----------	--	------

B, f, p	$\frac{dB}{B} = \gamma_{\text{tr}}^2 \frac{df}{f} + \frac{\gamma^2 - \gamma_{\text{tr}}^2}{\gamma^2} \frac{dp}{p}$	(25)
-----------	--	------

B, f, R	$\frac{dB}{B} = \gamma^2 \frac{df}{f} + (\gamma^2 - \gamma_{\text{tr}}^2) \frac{dR}{R}$	(26)
-----------	---	------

The index for the reference particle has been dropped since, e.g., $R = R_0 + \Delta R \simeq R_0$.

6.4.2 Application to energy matching

Each of the differential Eqs. (23) to (26) depends on three variables. It means that the choice of two parameters from the set B, p, R and f automatically constrains all others in both accelerators. By fixing, e.g., the bending field in a synchrotron, $dB = 0$, the revolution frequency with the radial position offset of the beam are linked directly by the relation

$$\gamma^2 \frac{df}{f} = (\gamma_{\text{tr}}^2 - \gamma^2) \frac{dR}{R}.$$

Without changing the magnetic field the beam can thus not circulate at the central orbit and at a given revolution frequency simultaneously. The bending field must be changed in this case to match it.

The energy matching of an incoming beam with respect to the expected energy in the receiving synchrotron can be verified by observing its revolution frequency during a de-bunching in combination with a measurement of radial position offset [36, 37]. Fig. 28 shows mountain range plots during the de-bunching during the first 1.8 ms after injection of a proton bunch into the PS at CERN. For this

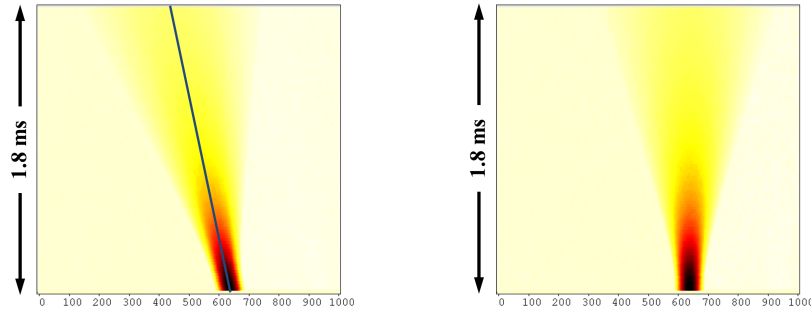


Fig. 28: De-bunching with an offset in bending field (left) and well matched (right).

transfer the revolution frequency in the PS and the radial position offset are kept constant. Hence the bending field and the momentum are defined according to Eqs. (23) to (26). The RF is switched off, but the triggers for the acquisitions of the beam signals are still derived from a synthesizer generating the reference revolution frequency for the transfer. In the left image the bunch centre advances with respect to the trigger corresponding to a too large revolution frequency. At the same time a radial position offset of the circulating beam after injection is measured. The energy of the incoming beam is therefore slightly too high. The beam circulates too far outside with a too high revolution frequency. After correction of

both, the bending field at injection and the momentum of the incoming bunch, the beam de-bunches exactly at the expected revolution frequency and at the central orbit, $\Delta R = 0$.

6.5 Longitudinal Matching

As shown above, the phase and the absolute energy of an incoming beam must match the position of the RF bucket, as well as the expected energy of the receiving accelerator. However, also the aspect ratio in terms of bunch length and energy spread of the injected bunch must be matched to the aspect ratio of the RF bucket to avoid longitudinal quadrupole oscillations and uncontrolled emittance growth.

The equations of motion (7) and (9) have the form of Hamilton equations for which the Hamiltonian can be written as [38]

$$H\left(\Delta\phi, \frac{\Delta E}{\omega_{\text{rev}}}\right) = -\frac{1}{2} \frac{h\eta\omega_{\text{rev}}}{pR} \left(\frac{\Delta E}{\omega_{\text{rev}}}\right)^2 + \frac{qV}{2\pi} [\cos(\phi_0 + \Delta\phi) - \cos\phi_0 + \Delta\phi \sin\phi_0]. \quad (27)$$

In the special case of small phase deviations $\Delta\phi \ll 1$, the potential term can again be approximated

$$\begin{aligned} \cos(\phi_0 + \Delta\phi) &= \cos\phi_0 \cos\Delta\phi - \sin\phi_0 \sin\Delta\phi \\ &\simeq \cos\phi_0 \left(1 - \frac{1}{2}\Delta\phi^2\right) - \sin\phi_0 \Delta\phi \end{aligned}$$

such that the Hamiltonian simplifies to

$$H\left(\Delta\phi, \frac{\Delta E}{\omega_{\text{rev}}}\right) \simeq -\frac{1}{2} \frac{h\eta\omega_{\text{rev}}}{pR} \left(\frac{\Delta E}{\omega_{\text{rev}}}\right)^2 - \frac{1}{2} \frac{qV}{2\pi} \Delta\phi^2 \cos\phi_0. \quad (28)$$

This approximated form of the Hamiltonian contains only quadratic terms of $\Delta\phi$ and ΔE . Consequently, it describes elliptical trajectories in the longitudinal E - ϕ -phase space.

The aspect ratio of the elliptical trajectories is evaluated by considering that, the Hamiltonian at the points of maximum phase or maximum energy deviation

$$\begin{aligned} H\left(\Delta\phi = 0, \frac{\Delta E}{\omega_{\text{rev}}}\right) &= -\frac{1}{2} \frac{h\eta\omega_{\text{rev}}}{pR} \left(\frac{\Delta E}{\omega_{\text{rev}}}\right)^2 \\ H\left(\Delta\phi, \frac{\Delta E}{\omega_{\text{rev}}} = 0\right) &= -\frac{1}{2} \frac{qV}{2\pi} \Delta\phi^2 \cos\phi_0 \end{aligned}$$

must be identical for a given trajectory such that

$$H\left(\Delta\phi = 0, \frac{\Delta E}{\omega_{\text{rev}}}\right) = H\left(\Delta\phi, \frac{\Delta E}{\omega_{\text{rev}}} = 0\right).$$

Replacing the phase $\Delta\phi$ by $\Delta\tau = 2\pi f_{\text{RF}} \Delta\tau = h\omega_{\text{rev}} \Delta\tau$ as a frequency independent variable and using

$$pR = \frac{E\beta^2}{\omega_{\text{rev}}},$$

Eq. (6.5) can be written as

$$-\frac{1}{2} \frac{h\eta\omega_{\text{rev}}^2}{E\beta^2} \left(\frac{\Delta E}{\omega_{\text{rev}}}\right)^2 = -\frac{1}{2} \frac{qV}{2\pi} h^2 \omega_{\text{rev}}^2 \Delta\tau^2 \cos\phi_0.$$

The aspect ratio $\Delta E/\Delta\tau$ of the elliptical trajectory finally becomes

$$\left(\frac{\Delta E}{\Delta\tau}\right)^2 = \frac{qV}{2\pi} E\beta^2 h\omega_{\text{rev}}^2 \frac{\cos\phi_0}{\eta}. \quad (29)$$

For a longitudinally matched transfer between two synchrotrons the parameters must be chosen such that the aspect ratios Eq. (29) are the same in both, sending and receiving, accelerators. This assures that the particle distribution in the longitudinal phase space can remain unchanged before and after the beam transfer. It results in the general longitudinal matching condition

$$q_1 V_1 E_1 \beta_1^2 h_1 \omega_{\text{rev},1}^2 \frac{\cos \phi_{0,1}}{\eta_1} = q_2 V_2 E_2 \beta_2^2 h_2 \omega_{\text{rev},2}^2 \frac{\cos \phi_{0,2}}{\eta_2}.$$

It is worth noting that matching is only perfect for small bunches in large buckets due to the approximation of the Hamiltonian.

In most cases the charge, velocity and energy of the particles do not change during the transfer. Most transfers take moreover place constant energy, with a synchronous phase, $\phi_{0,1}$ and $\phi_{0,2}$ of 0 or π , which simplifies the voltage ratio for a matched transfer to

$$\frac{V_1}{V_2} = \left(\frac{R_1}{R_2} \right)^2 \left| \frac{\eta_1}{\eta_2} \right| \frac{h_2}{h_1}. \quad (30)$$

The transfer between two synchrotrons where the receiving one operates at twice the RF frequency as the sending accelerator, $f_{\text{RF},2} = 2f_{\text{RF},1}$, is shown as an example for longitudinal matching. Figure 29 illustrates the combination of the longitudinal phase space in sending and receiving synchrotron. Even

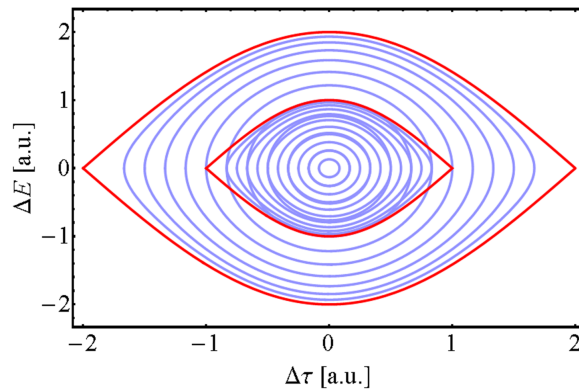


Fig. 29: Overlay of the longitudinal phase space in sending and receiving synchrotron.

though the bucket length and heights are very different, the inner trajectories of both buckets match very well. As long as the longitudinal emittance stays within that area, the transfer is longitudinally well matched.

6.5.1 Effect of voltage mismatch

Longitudinal mismatch at transfer leads to quadrupolar bunch oscillations, which is observed as a breathing of the bunch length, and to longitudinal emittance growth. The particle distributions obtained with single-particle tracking shown in Fig. 30 demonstrate this effect. While the matched distribution stays macroscopically unchanged (left), it rotates in the longitudinal phase space in the unmatched case (middle and right). Due to the non-linearity of the synchrotron frequency the bunch profile is massively perturbed. The filamentation finally leads to uncontrolled growth of the longitudinal emittance. While this emittance growth at transfer should be avoided for high-brightness beams, it may become a tool to deliberately reduce the longitudinal density for high-intensity beams. This technique is, e.g., used at injection of the anti-proton production beam into the PS at CERN [39].

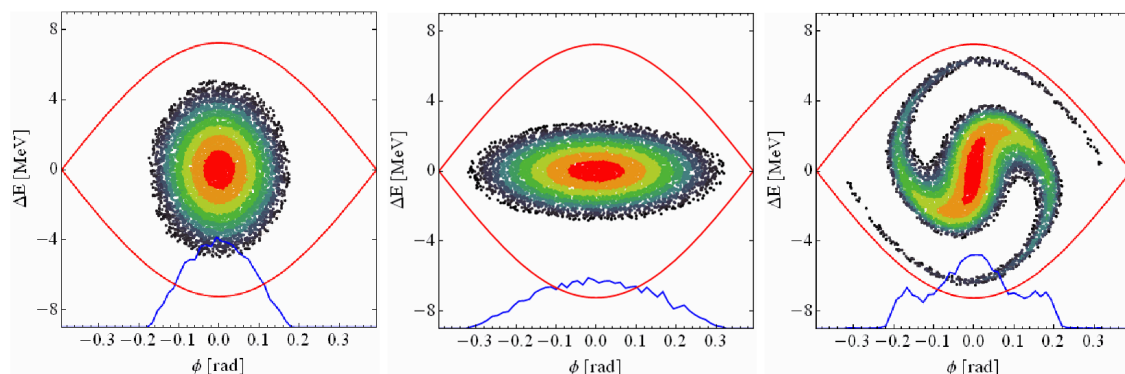


Fig. 30: Bunch distribution of a matched bunch after about 1.75 periods of the synchrotron frequency (left). Initial distribution of a longitudinally mismatched bunch (middle), and again after 1.75 periods of the synchrotron period.

6.5.2 Effect of bucket phase and energy mismatch

As discussed above also the bucket phase and energy of the RF bucket can be mismatched with respect to an incoming bunch. This can be seen in the simulated mountain range plots Fig. 31, where the RF bucket is displaced in phase (left) and energy (right). While the longitudinal phase space distribution

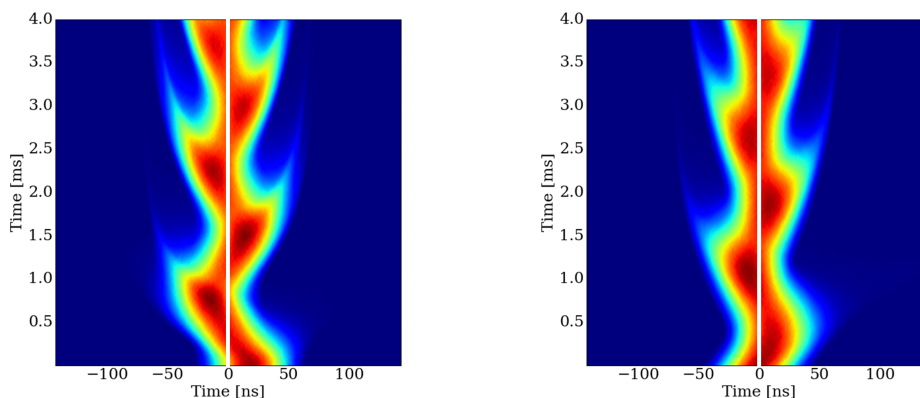


Fig. 31: Mountain range plot of bunch captured in a displaced RF bucket at injection. The initial displacement can be either in phase (left) or energy (right).

can only be accessed by tomographic techniques, the mountain range plots can be easily measured in a real accelerator. The phase error established at injection in the left plot is set to 45° and the energy error set for the simulation shown on the right plot also corresponds to the same oscillation amplitude. Qualitatively both images look very similar. However, the initial phase of the oscillation is different. With a pure phase error, the phase displacement with respect to the bucket center can be observed, which is not the case for an energy error. The mismatch (Fig. 31, left) can be corrected by changing the phase of the incoming bunch with respect to the RF bucket, while the energy error (Fig. 31, right) can only be removed by an energy matching (Sec. 6.4.2).

In electron accelerators, phase and energy mismatch can actually be used as a feature for special longitudinal injection schemes. For the electron option of the Future Circular Collider (FCC-ee), an off-momentum and off-phase injection is proposed [40]. Due to the strong synchrotron radiation the injected beam jumps the septum blade after one turn (Fig. 32). Thereafter it spirals toward the bucket centre at the reference energy. Similar schemes have been used for off-momentum injection and accumulation of beams into the Large Electron Positron collider (LEP) at CERN [41]. A first bunch was injected at an

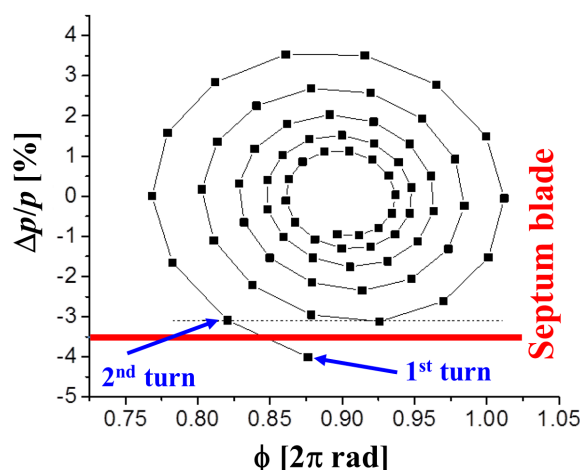


Fig. 32: Proposed synchrotron injection into FCC-ee. After the first turn, the injection bunch jumps the injection septum blade and then spirals towards the bucket centre.

energy slightly below the energy of the accumulated beam. After half a period of the synchrotron oscillation, the bunch moved to an energy above the reference energy, freeing the longitudinal phase space below for a second injection. This so-called double batch injection scheme again obviously only works for lepton bunches which match themselves to the buckets thanks to synchrotron radiation damping.

7 Acknowledgement

The author would like to thank Masamitsu Aiba, Maria-Elena Angoletta, Kalantari Babak, Diego Barrientos, Philippe Baudrenghien, Chandra Bhat, Thomas Bohl, Craig Drennan, Roland Garoby, Christopher Gough, Steven Hancock, Stephan Hunziker, Andreas Jankowiak, Boris Keil, Karim Lihem, John Molendijk, Holger Schlarb, Fumihiko Tamura, Frank Tecker, Daniel Valuch for discussions and material provided in preparation of this course.

References

- [1] H. Schlarb, *Timing and Synchronization*. In CERN Accelerator School: Advanced Accelerator Physics, Trondheim, Norway, 2015, available at the URL cas.web.cern.ch/sites/cas.web.cern.ch/files/lectures/trondheim-2013/schlarb.pptx.
- [2] Universität Bonn, *The Bonn University Electron Synchrotron*. In: CERN Symposium on High Energy Accelerators and Pion Physics, Geneva, Switzerland, 1956, pp. 482–483, <https://cds.cern.ch/record/1241624>.
- [3] M. Sands, *The Physics of Electron Storage Rings: An Introduction*. SLAC-R-121, University of California, Santa Cruz, California, USA, 1970 and revised, 1979, available at the URL <http://www-public.slac.stanford.edu/scidoc/docMeta.aspx?slacPubNumber=slac-R-121>.
- [4] H. Nyquist, *Thermal Agitation of Electric Charge in Conductors*. Physical Review, Vol. 32, 1928, pp. 110–113.
- [5] A. Van Der Ziel, *Thermal Noise at High Frequencies*. Journal of Applied Physics, Vol. 21, 1950, pp. 399–401.
- [6] IEEE, *IEEE Standard Definitions of Physical Quantities for Fundamental Frequency and Time Metrology-Random Instabilities*. IEEE Std 1139-1999, The Institute of Electrical and Electronics Engineers, Inc., New York, New York, USA, 1999.

- [7] G. Lutes et al., *Thermal Coefficient of Delay for Various Coaxial and Fiber-Optic Cables*. The Telecommunications and Data Acquisition Progress Report, TDA PR 42-99, Jet Propulsion Lab., California Inst. of Tech., Pasadena, California, USA, 1989, pp. 43-59, available at the URL <https://ntrs.nasa.gov/search.jsp?R=19900010123>.
- [8] J. Molendijk et al., *AWAKE - Status of the RF System*. AWAKE collaboration meeting, Lisbon, Portugal, 2016, available at the URL https://indico.cern.ch/event/484032/contributions/2002124/attachments/1240311/1825548/AwakeRF_Status_Lisbon.pdf.
- [9] D. Barrientos et al., *RF Synchronization and Distribution for AWAKE at CERN*. IPAC2016, Busan, Korea, 2016, pp. 3743–3746, available at the URL <http://accelconf.web.cern.ch/AccelConf/ipac2016/papers/thpmy039.pdf>.
- [10] A. Gallo, *Timing and Synchronization*. In: CERN Accelerator School: Advanced Accelerator Physics, Warsaw, Poland, 2015, available at the URL <cas.web.cern.ch/sites/cas.web.cern.ch/files/lectures/warsaw-2015/gallo.pdf>.
- [11] F. Loehl, *Timing and Synchronization*. In CERN Accelerator School: Advanced Accelerator Physics, Chios, Greece, 2011, available at the URL <cas.web.cern.ch/sites/cas.web.cern.ch/files/lectures/chios-2011/loehl.pdf>.
- [12] U. L. Rohde, *Microwave and Wireless Synthesizers: Theory and Design*. Wiley, New York, New York, USA, 1997.
- [13] R. Garoby, *Low level RF building blocks*. In: CERN Accelerator School: RF Engineering for Particle Accelerators, Oxford, United Kingdom, 1991, available at the URL <http://cds.cern.ch/record/225609>.
- [14] Hewlett Packard Company, *Model 10514A, B Mixers*. Operating and Service Manual, 1967.
- [15] Analog Devices, *AD834, 500 MHz Four-Quadrant Multiplier*. Data sheet, 2012.
- [16] W. T. Greer, *Digital phase-locked loops move into analog territory*. Electronic Design, 1982, pp. 95–100.
- [17] D. Abramovitch, *Phase-Locked Loops: A Control Centric Tutorial*. American Control Conference 2002, Anchorage, Alaska, USA, 2002.
- [18] Motorola, Inc. *MC12040, Phase-Frequency Detector*. Datasheet, 1997.
- [19] J. Volder, *The CORDIC Computing Technique*. Western Joint Computer Conference, Boston, Massachusetts, USA, 1959, pp. 257-261.
- [20] J. Kim et al., *Balanced optical–microwave phase detectors for optoelectronic phase-locked loops*. Optics Letters, Opt. Lett. 31, 3659-3661 (2006).
- [21] U. L. Rohde, J. C. Whitaker, H. Zahnd, *Communications receivers: Principles and Design*. McGraw-Hill Education, New York, New York, USA, 2017.
- [22] W. Pirkel, *Longitudinal Beam Dynamics*. In: CERN Accelerator School : 5th Advanced Accelerator Physics Course, Rhodes, Greece, 1995, available at the URL <https://cds.cern.ch/record/302486>.
- [23] G. Dôme, *Theory of RF Acceleration and RF Noise*. In: CERN Accelerator School: Antiprotons for Colliding-beam Facilities, CERN, Geneva, Switzerland, 1984, available at the URL <http://cds.cern.ch/record/863008>.
- [24] B. W. Montague, *Single-Particle Dynamics - RF Acceleration*. In: 1st International School of Particle Accelerators “Ettore Majorana” - Theoretical aspects of the behaviour of beams in accelerators and storage rings, CERN 77-13, Erice, Italy, 1977, available at the URL <https://cds.cern.ch/record/118362>.
- [25] D. Boussard, *Une présentation élémentaire du système Beam Control du PS*. MPS/SR/Note/73-10, CERN, Geneva, Switzerland, 1973.
- [26] D. A. G. Neet, *Timing for the ISR, Matching and Synchronization with the PS*. ISR-CO/67-28,

- CERN, Geneva, Switzerland, 1967, available at the URL <http://cds.cern.ch/record/296980>.
- [27] H. Damerau et al., *RF Manipulations for Higher Brightness LHC-Type Beams*. IPAC2013, Shanghai, China, 2013, pp. 2600-2602, available at the URL <http://accelconf.web.cern.ch/AccelConf/IPAC2013/papers/wepea044.pdf>.
- [28] R. Garoby, *Timing Aspects of Bunch Transfer Between Circular Machines, State of the Art in the PS Complex*. CERN/PS/RF/Note 84-6, CERN, Geneva, Switzerland, 1984, available at the URL <https://cds.cern.ch/record/2255149>.
- [29] R. Lauckner, *Matching the Energies of the CPS and SPS Machines*. SPS/AMS/Note/88-1, CERN, Geneva, Switzerland, 1988, available at the URL <http://cds.cern.ch/record/1065731>.
- [30] S. Hancock et al., *Single-batch Filling of the CERN PS for the LHC-type Beams*. IPAC2010, Kyoto, Japan, 2010, pp. 699-701, available at the URL <http://accelconf.web.cern.ch/AccelConf/IPAC10/papers/mopd014.pdf>.
- [31] A. V. Tollestrup, *R.F. Synchronization During Transfer in the Cascade Synchrotron*. Report CTSL-21, Synchrotron Laboratory, California Institute of Technology, Pasadena, California, USA, 1961, available at the URL <https://authors.library.caltech.edu/73330/>.
- [32] , W. Schnell, *Synchronization of ISR and CPS at Slightly Unequal Frequencies*. ISR-RF/66-18, CERN, Geneva, Switzerland, 1966.
- [33] T. Linnecar et al., *Hardware and Initial Beam Commissioning of the LHC RF Systems*. LHC Project Report 1172, CERN, Geneva, Switzerland, 2008, available at the URL <http://cds.cern.ch/record/1176380>.
- [34] C. Bovet et al., *A selection of formulae and data useful for the design of A.G. synchrotrons*. CERN-MPS-SI-INT-DL-70-4, CERN, Geneva, Switzerland, 1970, available at the URL <http://cds.cern.ch/record/104153>.
- [35] S. Hancock, *Transition revisited*. CERN/PS/90-53 (OP), CERN, Geneva, Switzerland, 1990.
- [36] S. Hancock et al., *A Straightforward Procedure to achieve Energy Matching Between PSB and PS*. CERN-AB-Note-2008-042, CERN, Geneva, Switzerland, 2008, available at the URL <http://cds.cern.ch/record/1125475>.
- [37] S. Hancock, *Energy Matching Between LEIR and PS*. CERN-ACC-NOTE-2015-0019, CERN, Geneva, Switzerland, 2015, available at the URL <http://cds.cern.ch/record/2038693>.
- [38] F. Tecker, *Longitudinal Beam Dynamics - Recap*. These proceedings.
- [39] H. Damerau et al., *Controlled Longitudinal Emittance Blow-up in the CERN PS*. PAC07, Albuquerque, New Mexico, USA, 2007, pp. 4186–4188, available at the URL <http://accelconf.web.cern.ch/AccelConf/p07/PAPERS/FRPMN070.PDF>.
- [40] M. Aiba, *Top-up injection for FCC-ee*. CERN-ACC-2015-065, CERN, Geneva, Switzerland, 2015, available at the URL <https://cds.cern.ch/record/2031423>.
- [41] R. Bailey, *Is Injection Up To Scratch for All Filling Scenarios?*. 6th LEP Performance Workshop, Chamonix, France, 1996, pp. 41–44, available at the URL http://sl-div.web.cern.ch/sl-div/publications/chamx96/papers/rb2_01.pdf.